Supporting Information

Enhancing Photocatalyst Stability for Hydrogen Peroxide Synthesis through Promoting Oxygen-Centered Organic Radical Formation

Pan Jiang[1], Zuoming Chen[1], Huijie Yan[1], Shufang Liu[1], Yuyan Huang[2], Xiangqiong Jiang[2], Xin Wu[1], Xiantai Zhou[1], Yu-Xin Ye[1,3]* & Gangfeng Ouyang[1,2,3]*

1 P. Jiang, Z. Chen, H. Yan, S. Liu, Dr. Y. -X. Ye, Prof. G. Ouyang
School of Chemical Engineering and Technology, ICGME
Sun Yat-sen University
Zhuhai 519082 (P. R. China)

2 Y. Huang, X. Jiang, Prof. G. Ouyang
Key laboratory of Bioinorganic and Synthetic Chemistry of Ministry of Education, LIFM, School of Chemistry, IGCME
Sun Yat-sen University
Guangzhou 510006 (P. R. China)

3 Dr. Y. -X. Ye, Prof. G. Ouyang
Southern Marine Science and Engineering Guangdong Laboratory (Zhuhai)
Zhuhai, Guangdong 519082 (P. R. China)

*Corresponding Author(s): yeyuxin5@sysu.edu.cn; cesoygf@mail.sysu.edu.cn

1. EXPERIMENTAL SECTION

1.1. Materials

3,5-Dibromotoluene (98%), N-bromosuccinimide (NBS, 99%), and sodium methanesulfinate (95%) were purchased from Aladdin Industrial Corporation and used as received. 3,5-Dibromoethylbenzene (97%), 2,6-Dibromoanthraquinone (97%), Cuprous iodide (CuI, 99%), 2,2-azobisisobutyronitrile (AIBN, 98%), Bis(triphenylphosphine)palladium(II) chloride ($Pd(PPh_3)Cl_2$, 98%), (triisopropylsilyl)acetylene (97%), tetrabutylammonium (TBAF, 98%), Tetrahydrofuran (THF, 99.9%, Extra Dry), Piperidine (98%), Acetonitrile (CH_3CN, 99.9%, Extra Dry) and N, N-dimethylformamide (DMF, 99.8%, Extra Dry) were purchased from Energy Chemical company and used as received. All other reagents and solvents were used directly without further purification. The actual water samples were collected from the Pearl River and the Center Lake.

1.2. Characterization

PXRD data was collected by D-MAX 2200 VPC. SEM images were obtained by SU8010. TEM images were performed on JEM-2010. Solid-state ^{13}C NMR spectroscopy was conducted using the Bruker AVANCE 600 MHz. Fourier transform infrared spectroscopy (FT-IR) data was collected using the Perkinelmer Frontier spectrometer. X-ray photoelectron spectroscopy (XPS) measurements were obtained using the Thermo Scientific Nexsa, with Al Kα radiation as the excitation source. Solid state UV-vis diffuse reflectance spectra were measured on a Shimadzu UV-3600 spectrometer. Photoelectron chemical and electrochemical measurements were performed using a CHI 760E Instruments electrochemical workstation. Photoluminescence (PL) spectra were measured on an FLS 1000 spectrophotometer. Electron paramagnetic resonance (EPR) signals were measured using a Bruker A 300 spectrometer. In-situ diffuse infrared Fourier-transform spectroscopy was determined using a German Bruker INVENIO S spectrometer equipped with an MCT detector, Harrick diffuse reflection in-situ cell, and a 300 W xenon lamp with a visible light filter.

1.3. Determination of H_2O_2 concentration

Preparation of HRP solution: First, 0.002 g of horseradish peroxidase (HRP) was dissolved in 10ml of deionized water.

Preparation of TMB solution: Specifically, 0.02 g ethylenediamine tetraacetic acid (EDTA) and 0.095 g citric acid were added to a mixture of 5 mL glycerin and 45 mL deionized water. 0.3 mL of DMSO containing 0.015 g of 3,3',5,5' -tetramethylbenzidine (TMB) was added to the aforementioned solution, and finally deionized water was added to make a total volume of 50 mL.

Finally, HRP and TMB solutions were mixed. The concentration of H_2O_2 was determined by UV-VIS spectrophotometry. The reaction of H_2O_2 with TMB was as follows：

$$H_2O_2 + \mathrm{T}MB \xrightarrow{HRP} H_2O + axTMB$$

The calibration curve was prepared by adding TMB and HRP into the known concentration of H_2O_2 solution, adding 10 μL HCl 3 min later, and performing UV-vis spectroscopy determination at 450 nm. Based on the linear relationship between signal intensity and H_2O_2 concentration, the standard calibration curve was used for the quantitative determination of H_2O_2 concentration.

1.4. Photoelectrochemical and electrochemical measurements

All materials were prepared by adding 5 mg of catalyst into the solution containing 180 μL of ethanol and 20 μL of 5% Nafion. The mixture was dispersed through ultrasonication.

All measurements were conducted on a three-electrode cell system of the electrochemical workstation (CHI 760E instrument). The standard three-electrode system consists of a working electrode, Ag/AgCl (saturated KCl) as the reference electrode, and a

Pt mesh as the counter electrode. A 300 W Xe lamp was employed as the illumination source. Mott-Schottky measurements and photocurrents were both conducted in 0.1 M sodium sulfate solution. The specific operation was to drop the mixture onto a glassy carbon electrode (for electrochemical impedance spectroscopy) or FTO glass (for Mott-Schottky and photocurrent tests), and the solvent was naturally evaporated in air.

The electron transfer number of the oxygen reduction reaction was tested on a rotating disk electrode (RDE) after bubbling oxygen for 30 minutes, with 0.1 M phosphate buffer solution as the electrolyte. The corresponding average electron transfer number was calculated using the Koutecky-Levich equation：

$$\frac{1}{J}=\frac{1}{J_L}+\frac{1}{J_K}=\frac{1}{B\omega^{1/2}}+\frac{1}{J_K}$$

$$B=0.2nFV^{-1/6}CD^{2/3}$$

Where J denotes the measured current density, J_K refers to the kinetic current density, J_L represents the limiting diffusion current density, ω represents the angular velocity, n is the transfer electron number, F stands for the Faraday constant (96485 C·mol^{-1}), V is the kinetic viscosity of water (0.01 cm^2·s^{-1}), C is the saturated oxygen concentration in the electrolyte (1.26×10^{-3} mol·L^{-1}), and D is the diffusion coefficient of O_2 (2.7 ×10^{-5}cm^2·s^{-1}).

1.5. AQY measurement of H_2O_2 Production

The apparent quantum yield (AQY) was determined under a multichannel light panel equipped with multiple single-wavelength LEDs (CEL-LEDS35). The photocatalytic reaction was measured by adding the photocatalyst (10 mg) into a quartz tube containing pure deionized water (50 mL). The tube was irradiated with an LED lamp for 1 hour under magnetic stirring. The number of incident photons (M) was calculated as follows:

$$M=\frac{E\lambda}{hc}$$

In the equation, E represents the average irradiation intensity, λ represents the irradiation wavelength, h is the Planck constant, and c represents the speed of light. The calculation equation of quantum efficiency is as follows:

$$AQY=\frac{2\times number\ of\ elvoved\ H_2O_2\ molecules}{number\ of\ incident\ photons}\times 100\%$$

1.6. Solar-to-chemical conversion (SCC) efficiency

The SCC efficiency was determined with the photocatalyst (100 mg) dispersed in pure deionized water (100 mL), employing an AM 1.5 G solar simulator as the light source (100 mW·cm^{-2}). The photoreaction was conducted in a glass bottle and the irradiation area was 1 × 10^{-4} m^2. The SCC efficiency (η) was calculated by the following equation:

$$SCC=\frac{\triangle GH_2O_2\times nH_2O_2}{t_{ir}\times S_{ir}\times I_{AM}}\times 100\%$$

where ΔGH_2O_2 is the free energy for H_2O_2 generation (117 kJ mol^{-1}, nH_2O_2 is the amount of H_2O_2 generated, and t_{ir} is the irradiation time (3600 s). I_{AM} and S_{ir} represent the irradiation intensity and area.

1.7. Electron paramagnetic resonance (EPR) measurements

Spin trapping-EPR tests were recorded using a Bruker A300 spectrometer. 5,5-dimethyl-1- pyrroline N-oxide (DMPO) were used as a spin-trapping reagents to detect $O_2^{\bullet-}$. The samples were prepared by adding 0.5 mg catalysts into 200 μL methanol containing the trapping agents. Light induced EPR signals were collected using a 300 W Xenon lamp.

The in-situ EPR tests for the investigation of OCORs were also carried on the Bruker A300 Electron Paramagnetic Resonance. A specific quantity of solid catalysts was loaded into a capillary, sealed it after purging with argon and exposed it to light for a certain duration. EPR signals were recorded at regular intervals. The decay process of the EPR signals was recorded subsequently after removing the visible light irradiation.

1.8. TAS Measurements

The TA spectra of CPs were measured using the Helios femtosecond transient absorption spectrometer (Ultrafast Systems, LLC). A 400-nm pump pulse, generated by an optical parametric amplifier (OPerA Solo, Coherent), had a laser intensity of 150 μW. The sample was prepared in the following way: 10 mg of the photocatalyst was dispersed in 20 mL of deionized water. Then the suspension underwent ultrasonic treatment for 36 hours. The initial suspension was centrifuged at 3000 rpm for 10 minutes to eliminate large aggregates. The supernatant was extracted for subsequent detection. To identify the observed signal, electron ($AgNO_3$) and hole (EDTA-2Na) sacrificial agents (10 mM) were added to the supernatant.

1.9. Stability cycling assessment

30 mg of the catalyst was incorporated into 50 mL of pure water, subjected to ultrasonic dispersion for 30 minutes, stirred and illuminated with xenon light for 1 hour, with the light intensity regulated at 100 mW/cm^2. Subsequently, it was subjected to suction filtration and drying. Thereafter, 1 mg was weighed out, introduced into 50 mL of pure water, underwent ultrasonic dispersion for 30 minutes, was stirred and irradiated with xenon light for one hour for performance testing. Such tests were repeated iteratively.

1.10. Oxidation experiment of NBT

1 mg of the prepared catalyst was suspended in 50 mL of NBT aqueous solution and irradiated with a xenon lamp. Before irradiation, it was continuously stirred in the dark for 30 min. After the reaction ended, 3 mL of the reaction suspension was taken. The photocatalyst was separated by centrifugation, and the absorbance of the supernatant was recorded on a UV-Vis spectrophotometer (Shimadzu UV-3600 spectrometer). The photocatalytic generation of $\cdot O_2^-$ was determined by the degradation of NBT, which was monitored by the change in absorbance at a wavelength of 259 nm.

The superoxide radical produced was calculated according to the following formula:

$$NBT + 4 \cdot O_2^- + H^+ \rightarrow Formazan + 4O_2$$

1.11. Density Functional Theory (DFT) Calculation

The DFT calculations were conducted in the Gaussian 09 D.01 program package with Grimme-D3 dispersion correction.[1] GaussView5 was employed for visualization. The geometries of simplified fragments of the catalysts were performed by method B3LYP/6-31G**. There are no imaginary frequencies for all optimized structures.[2-3] Time-dependent density functional theory (TD-DFT) was calculated at pbe1pbe/6-31G (d,p) level of theory and was used to investigate the transfer direction of electrons.[4] Multiwfn was used for hole-electron analysis.[5-6]

2. Synthesis of TMS-AQ, AQ, SF-TIPS, SF-H

2.1. Preparation of AQ monomer：

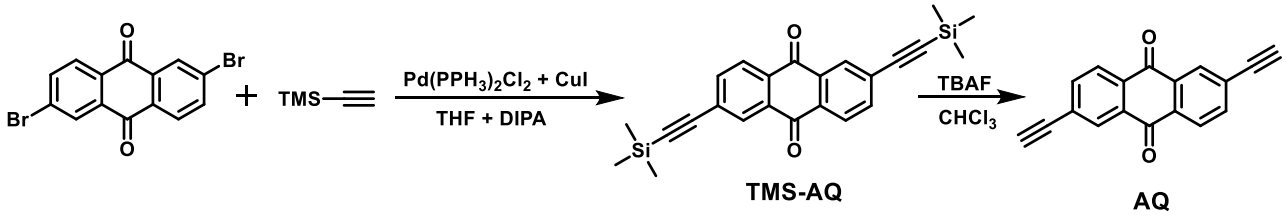

Scheme S1. Synthetic routes of the **TMS-AQ** and **AQ**.

The synthetic method reported in the reference literature：

*(1) Synthesis of 2,6-bis((trimethylsilyl)ethynyl)anthracene-9,10-dione（**TMS-AQ**）*

The synthesis of **TMS-AQ** was carried out by adding 2,6-dibromoanthraquinone (1830 mg, 5 mmol), copper(I) iodide (9.5 mg, 0.05 mmol), bis(triphenylphosphine)palladium(II) chloride (35.1 mg, 0.05 mmol), tetrahydrofuran (70 mL), and diisopropylamine (70 mL) to a 250 mL round-bottom flask. Under an argon atmosphere, 20 mmol of trimethylsilylacetylene was added, and the mixture was heated and stirred at 80°C for 24 hours. After completion of the reaction, the mixture was cooled to room temperature, and the solvent was removed by vacuum distillation using a rotary evaporator. The crude product was purified by column chromatography using a mixture of 3/1 (v/v) petroleum ether/dichloromethane as the eluent, yielding a pale yellow solid with a yield of approximately 50%.[7]

*(2) Synthesis of 2,6-diethynylanthraquinone （**AQ**）*

Compound **TMS-AQ** (0.5 mmol) was dissolved in 10 mL of chloroform, and then a solution of tetrabutylammonium fluoride (70%, 0.62 g) was slowly added dropwise to the above solution with stirring. After complete addition, stirring was continued at room temperature for 30 minutes, and then 10 mL of deionized water was added to the mixture.

The organic layer was washed three times with saturated sodium chloride solution and deionized water by liquid-liquid extraction. The solvent was removed by vacuum distillation, and the solid product was washed with methanol and filtered. Finally, the solid product was vacuum dried to yield a yellow solid with a yield of about 93%.[7]

2.2. Synthesis of ((5-((methylsulfonyl)methyl)-1,3-phenylene)bis(ethyne-2,1-diyl))bis(triisopropylsilane) (**SF-TIPS**) and 1,3-diethynyl-5-((methylsulfonyl)methyl)benzene (**SF-H**)

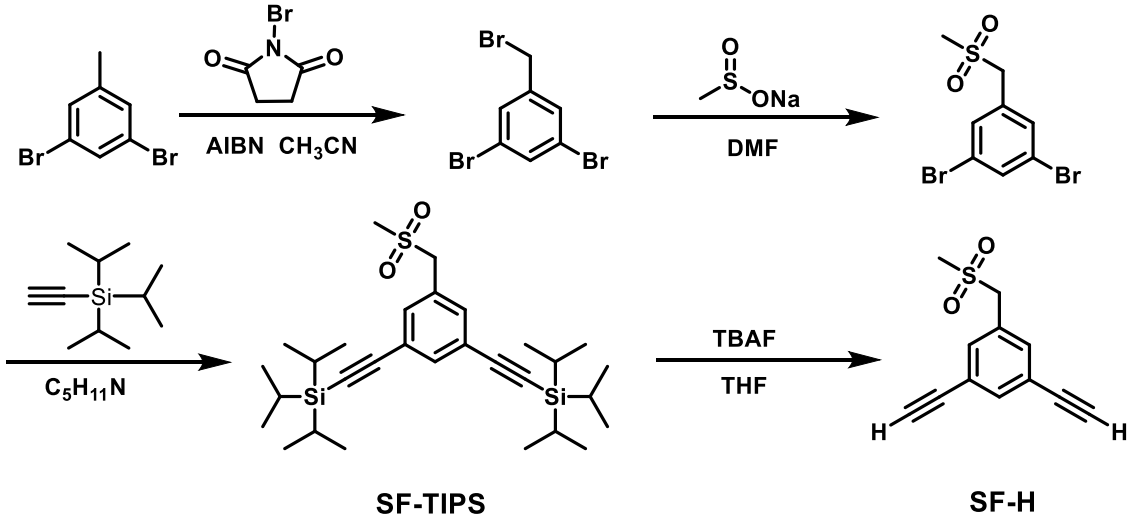

Scheme S2. Synthetic routes of the **SF–TIPS** and **SF-H**.

(1) Synthesis of 1,3-dibromo-5-(bromomethyl) benzene

The synthesis method reported in the reference literature: 3,5-Dibromotoluene (10 g, 40.08 mmol), NBS (7.12 g, 40.08 mmol), AIBN (0.33 g, 2 mmol), dissolved in acetonitrile (120 ml), heated under argon protection to 85°C and refluxed for 3 hours. After cooling to room temperature, the mixture was rotary evaporated, and the residue was purified by petroleum ether column chromatography to yield 7.2 g of white crystals, with a yield of 53.8%.[8]

(2) Synthesis of 1,3-dibromo-5-((methylsulfonyl) methyl) benzene

The synthesis method reported in the reference literature: 1,3-dibromo-5-(bromomethyl)benzene (5 g, 15.21 mmol) and sodium methanesulfinate (3.74 g, 36.6 mmol) were added to DMF (50 mL) and reacted at 70°C for 3 hours. The mixture was then cooled to room temperature, precipitated in saturated NaCl aqueous solution, filtered, and dried to yield 4.8 g of white product, with a yield of 95%.[8]

^{1}H NMR (400 MHz, DMSO-d_6) δ 7.88 (t, J=4 Hz, 1H), 7.67 (d, J=4 Hz, 2H), 4.58 (s, 2H), 2.97 (s, 3H). ^{13}C NMR (101 MHz, DMSO-d_6) δ 134.20, 133.81,133.23, 122.79, 58.26.

*(3) Synthesis of ((5-((methylsulfonyl)methyl)-1,3-phenylene)bis(ethyne-2,1-diyl))bis(triisopropylsilane) (**SF–TIPS**)*

1,3-dibromo-5-((methylsulfonyl) methyl) benzene (1.058 g, 3.2mmol), triisopropylsilylacetylene (1.411 g, 8.1 mmol), bis(triphenylphosphine)palladium dichloride (22 mg, 0.3 mmol), and cuprous iodide (61 mg, 0.32 mmol) were dissolved in pyridine

(100 mL). The mixture was heated to 70°C under argon atmosphere and kept for 24 hours, then cooled to room temperature and rotary evaporated. The crude product was purified by column chromatography on dichloromethane to afford 1.54 g of pale yellow solid, with a yield of 95%.

^{1}H NMR (400 MHz, DMSO-d_6) δ 7.55 (d, J=4 Hz, 2H), 7.50 (t, J=4 Hz, 1H), 4.56 (s, 2H), 2.95 (s, 3H), 1.10 (42H). ^{13}C NMR (101 MHz, DMSO-d_6) δ 134.98, 134.41, 131.13, 123.52, 105.77, 92.08, 58.42, 18.95, 11.13.

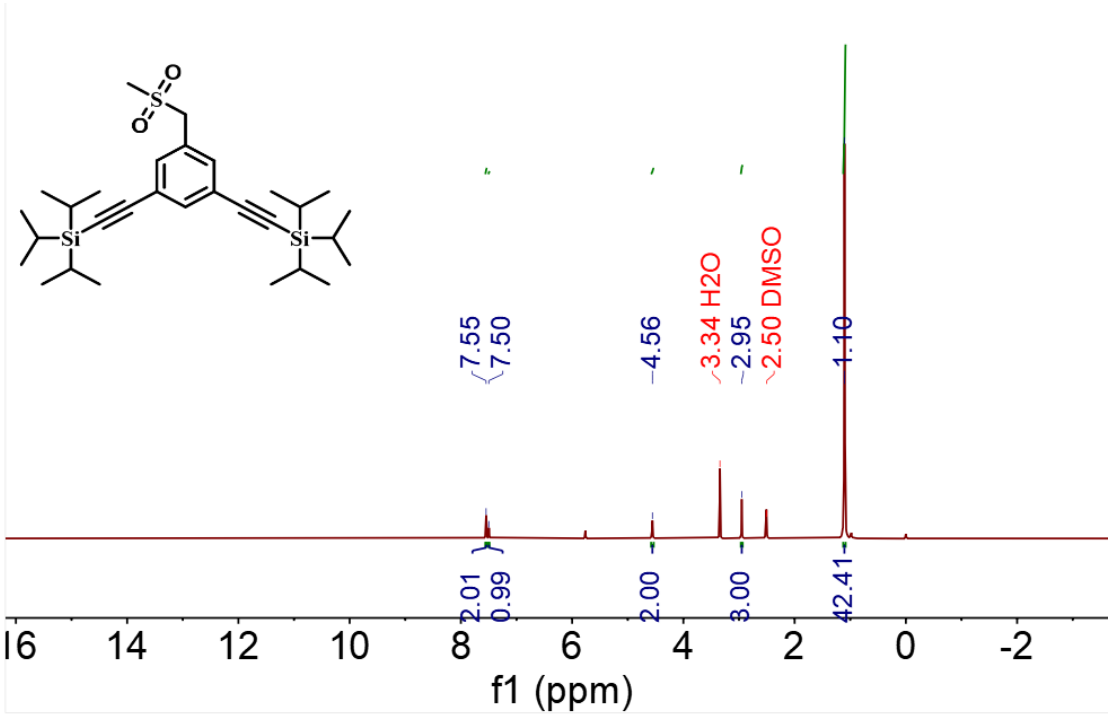

Figure S1. ^{1}H NMR (400 MHz, DMSO-d_6, 298 K) spectrum of **SF–TIPS**.

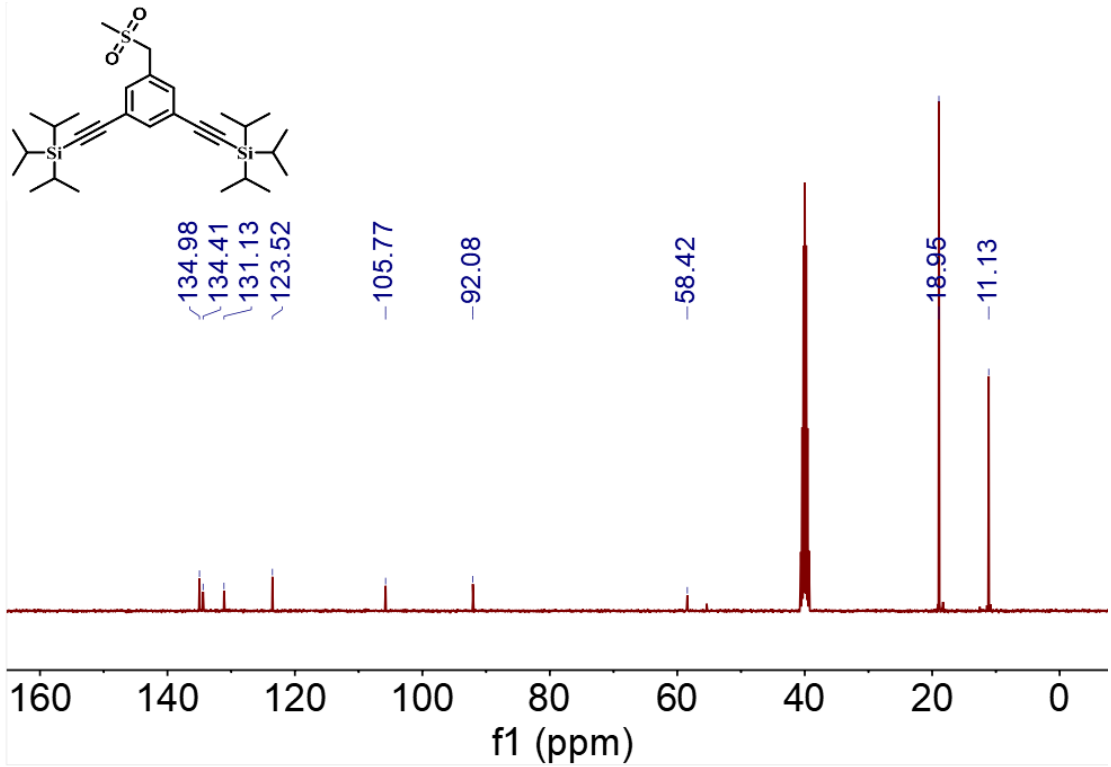

Figure S2. ^{13}C NMR (101 MHz, DMSO-d_6, 298 K) spectrum of **SF–TIPS**.

*(4) Synthesis of 1,3-diethynyl-5-((methylsulfonyl)methyl)benzene (**SF-H**)*

SF–TIPS (2.09 g, 4 mmol) was dissolved in tetrahydrofuran (50 ml), and then dropwise

added to a solution of tetrabutylammonium fluoride (5.14 g, 19.6 mmol) in an ice bath. The reaction mixture was stirred for half an hour, then evaporated to dryness under reduced pressure. The resulting residue was purified by column chromatography using dichloromethane to yield a yellow solid (0.85 g, 93% yield).

^{1}H NMR (400 MHz, DMSO-d_6) δ 7.58 (t, J=4 Hz, 1H), 7.55 (d, J=4 Hz, 2H), 4.53 (s, 2H), 4.35 (s, 2H), 2.93 (s, 3H). ^{13}C NMR (101 MHz, DMSO-d_6) δ 134.95, 134.75, 131.11, 123.00, 82.70, 82.35, 55.65.

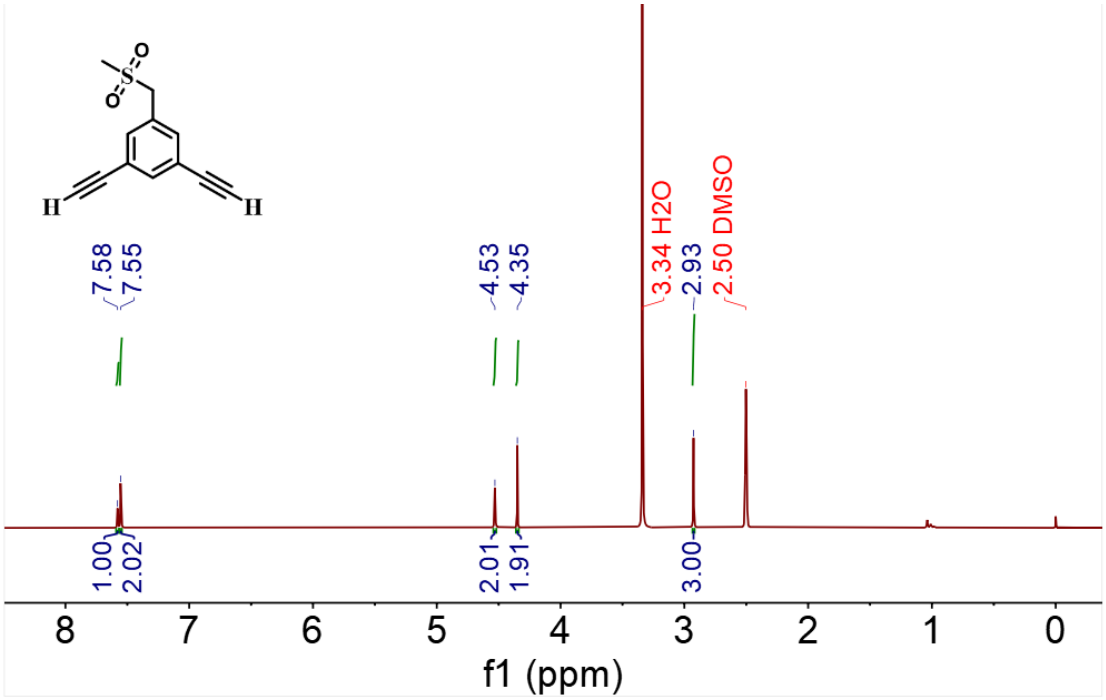

Figure S3. ^{1}H NMR (400 MHz, DMSO-d_6, 298 K) spectrum of **SF-H**.

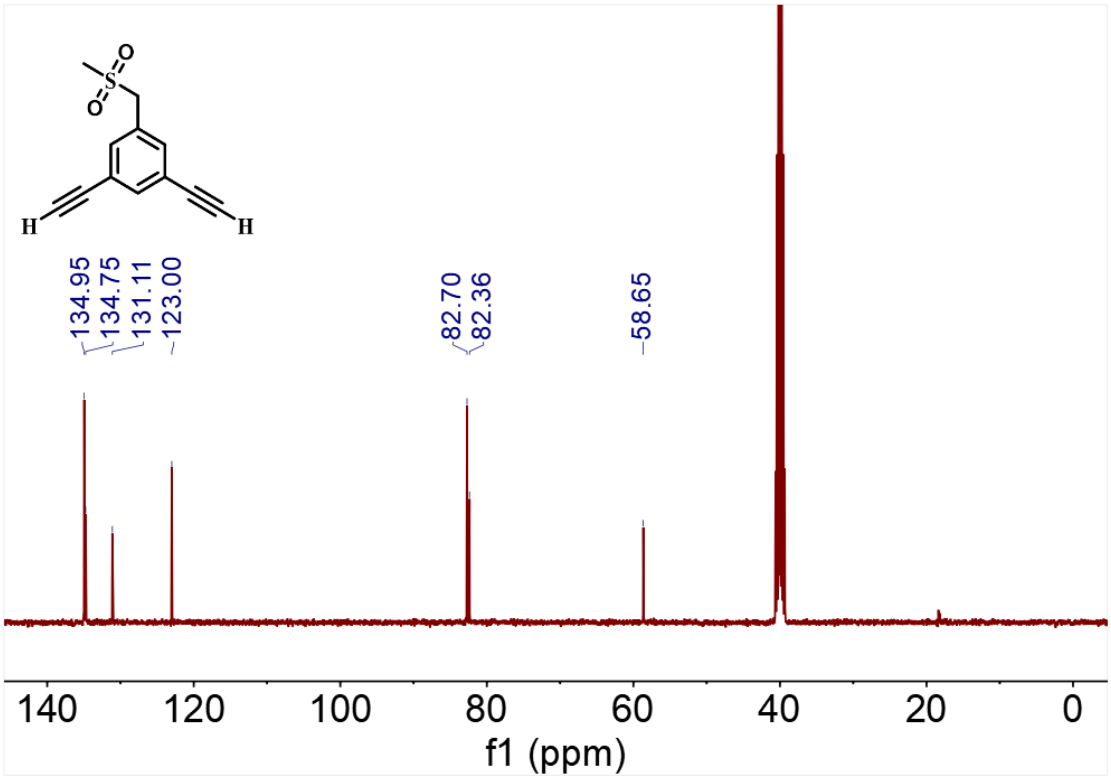

Figure S4. ^{13}C NMR (101 MHz, DMSO-d_6, 298 K) spectrum of **SF-H**.

2.3. Synthesis of compound Sulfonyl-AQ

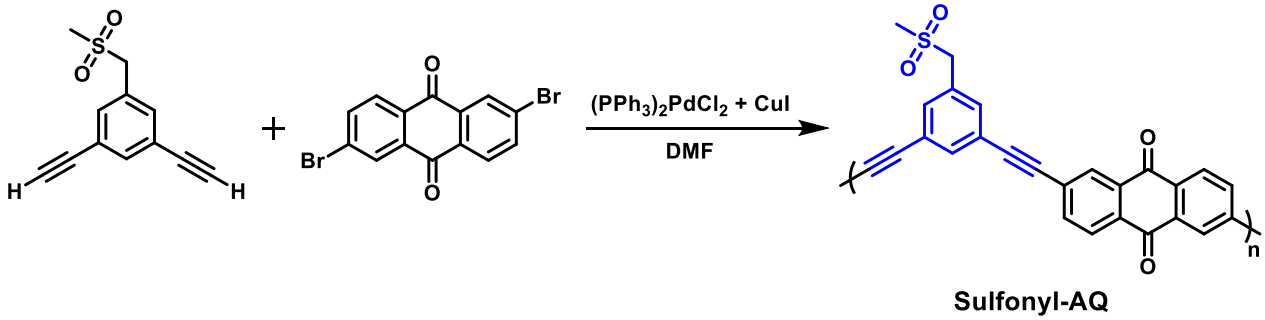

Scheme S3. Synthetic route of the **Sulfonyl-AQ**.

SF-H (64 mg) and 2,6-dibromoanthraquinone (50 mg) were dissolved in 50 mL of dimethylformamide (DMF) under an argon atmosphere. To the solution, $(PPh_3)_2PdCl_2$ (13 mg), CuI (3.71 mg), and triethylamine (50 mL) were added. The reaction mixture was stirred at 80°C for 48 hours. After cooling, the catalyst was obtained by sonication in DMF for 30 minutes, followed by centrifugation and washing with ethanol by sonication three

times. The catalyst was then filtered and dried at 60°C.

2.4. Synthesis of compound Ethyl-AQ

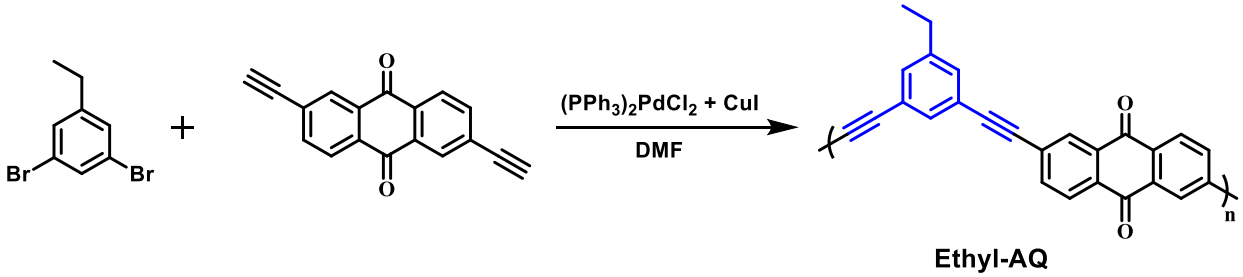

Scheme S4. Synthetic routes of the **Ethyl-AQ**.

54 mg of 3,5-dibromoethylbenzene and 50 mg of **AQ** were added to 50 mL of DMF under an argon atmosphere. To the solution, $(PPh_3)_2PdCl_2$ (13 mg), CuI (3.71 mg), and triethylamine (50 mL) were added. The reaction mixture was stirred at 80°C for 48 hours. After cooling, the catalyst was obtained by sonication in DMF for 30 minutes, followed by centrifugation and washing with ethanol by sonication three times. The catalyst was then filtered and dried at 60°C.

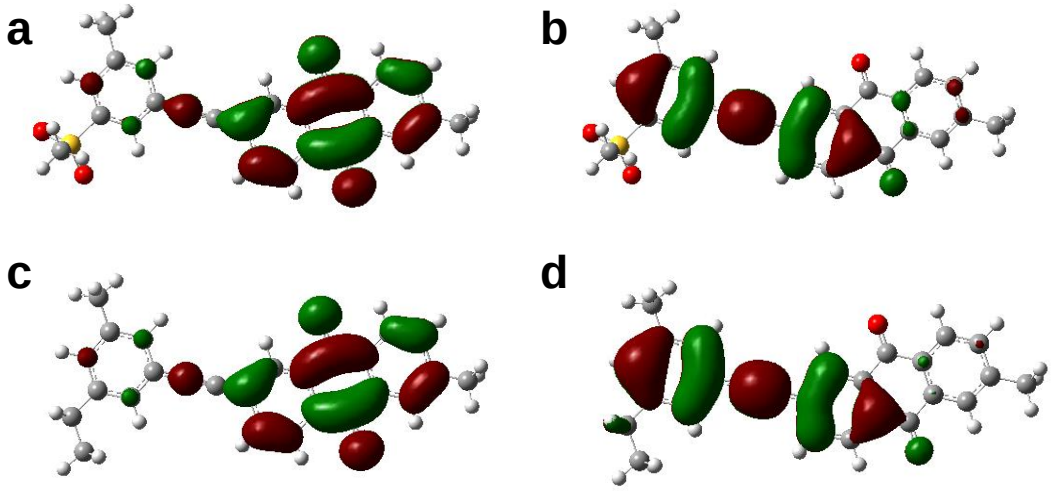

Figure S5. The lowest unoccupied molecular orbital (LUMO) diagrams of (a) Sulfonyl-AQ and (c) Ethyl-AQ. The highest occupied molecular orbital (HOMO) diagrams of (b) Sulfonyl-AQ and (d) Ethyl-AQ.

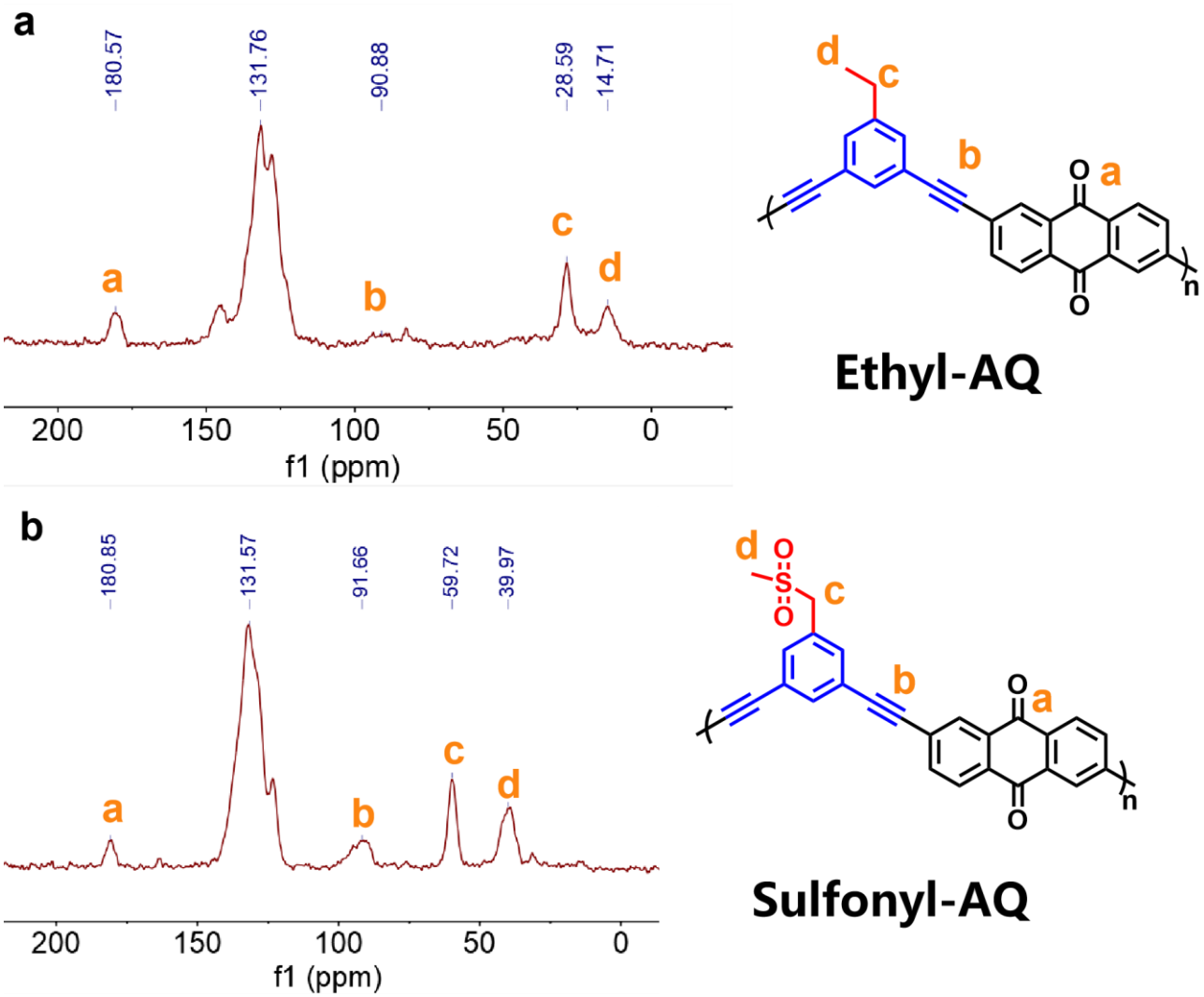

Figure S6. Solid-state ^{13}C NMR spectra of (a) Ethyl-AQ and (b) Sulfonyl-AQ.

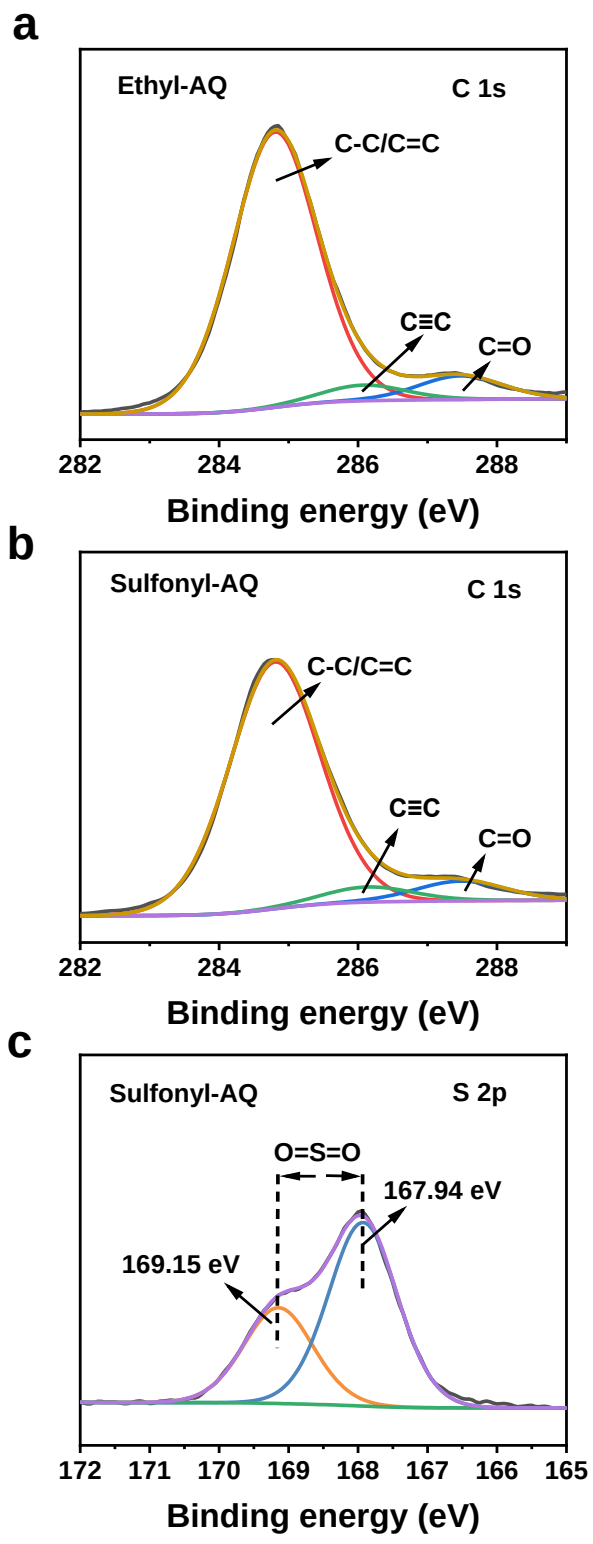

Figure S7. XPS spectra of Ethyl-AQ (a), Sulfonyl-AQ (b) for C 1s and (c) for S 2p.

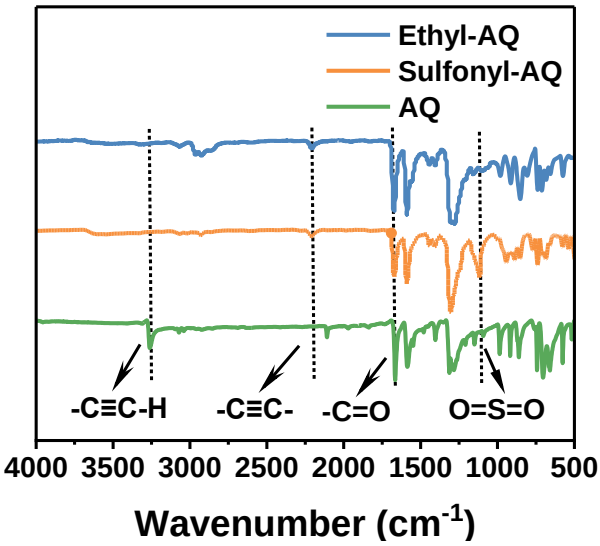

Figure S8. FT-IR spectra of CPs and anthraquinone monomer. The peak corresponding to the alkyne hydrogen's stretching vibration emerged at ≈3260 cm^{-1} in the anthraquinone monomer. It vanished in the CPs, suggesting the successful coupling of the alkyne with the electron donor and acceptor.

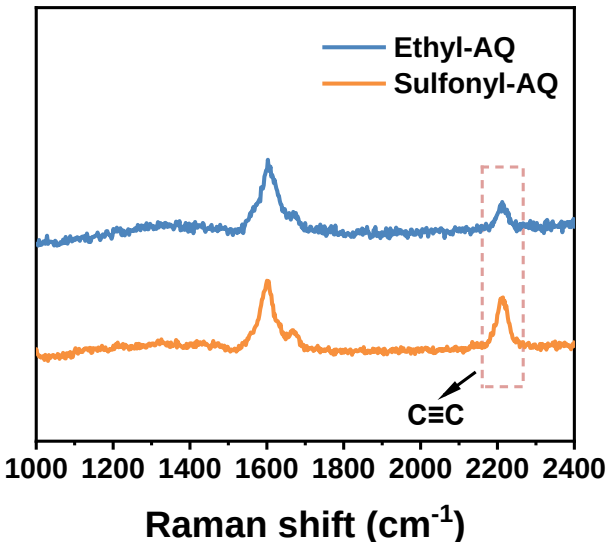

Figure S9. Raman spectra of Ethyl-AQ and Sulfonyl-AQ.

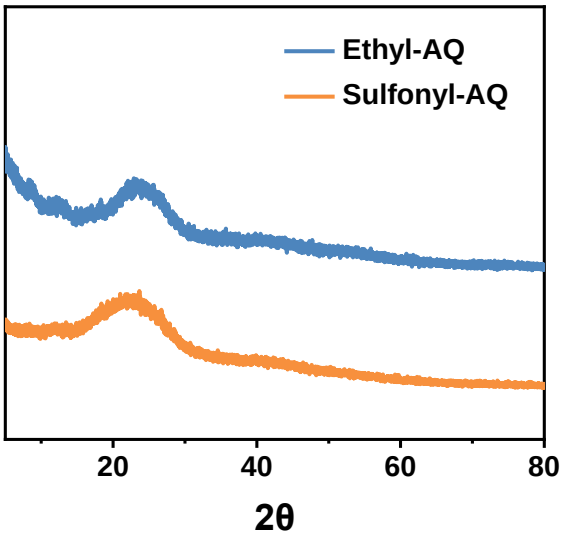

Figure S10. The PXRD characterization for CPs.

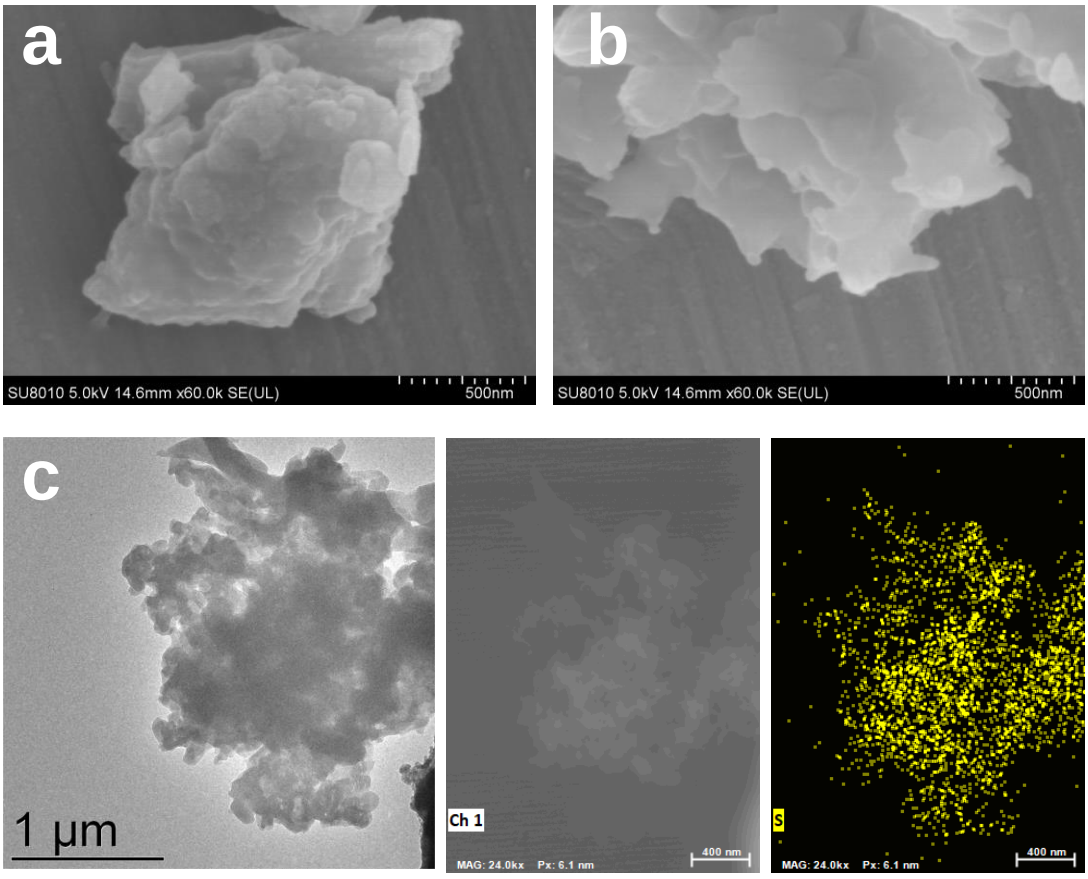

Figure S11. SEM images of Ethyl-AQ (a) and Sulfonyl-AQ (b); TEM image of Sulfonyl-AQ and its energy dispersive spectroscopy (EDS) mapping images (c).

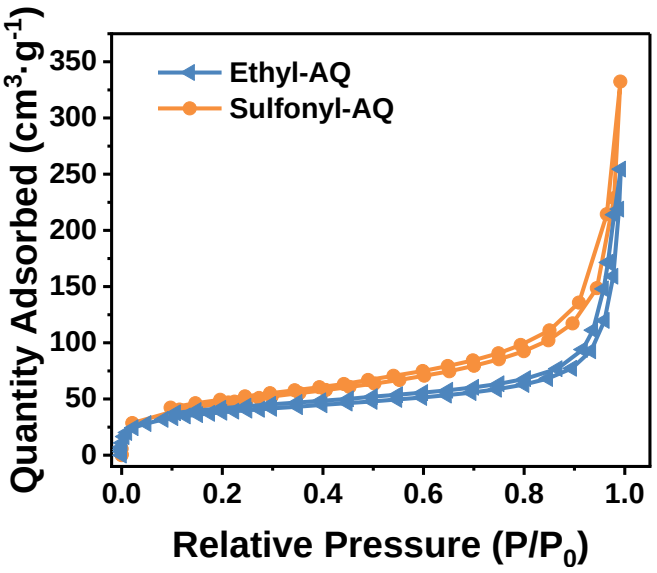

Figure S12. N_2 adsorption-desorption isotherms of Ethyl-AQ and Sulfonyl-AQ.

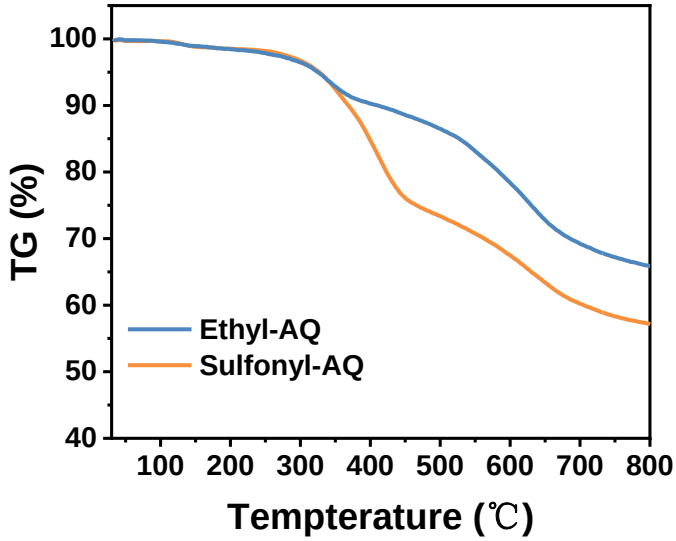

Figure S13. TG curves of Ethyl-AQ and Sulfonyl-AQ under N_2 atmosphere.

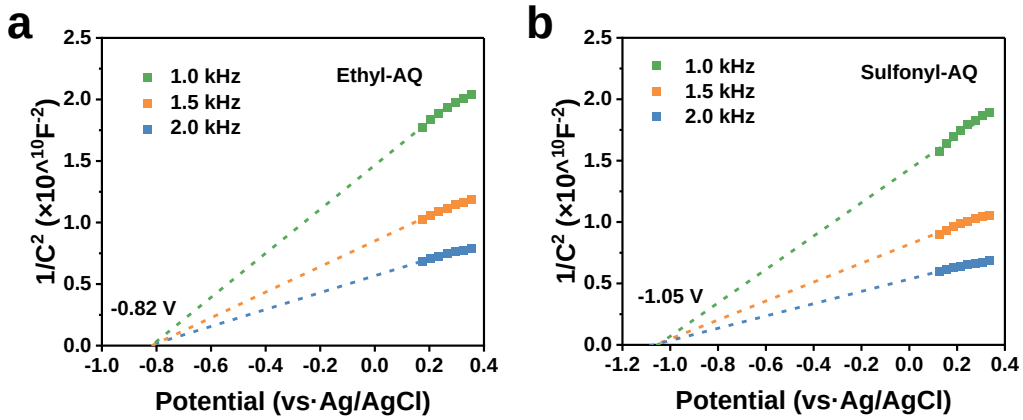

Figure S14. Mott-Schottky plots of (a) Ethyl-AQ, (b) Sulfonyl-AQ for characterizing

conduction band (CB). The conduction band (CB) minima for Ethyl-AQ and Sulfonyl-AQ were determined to be -0.21 eV and -0.44 eV versus the reversible hydrogen electrode (RHE) via the Mott-Schottky tests.

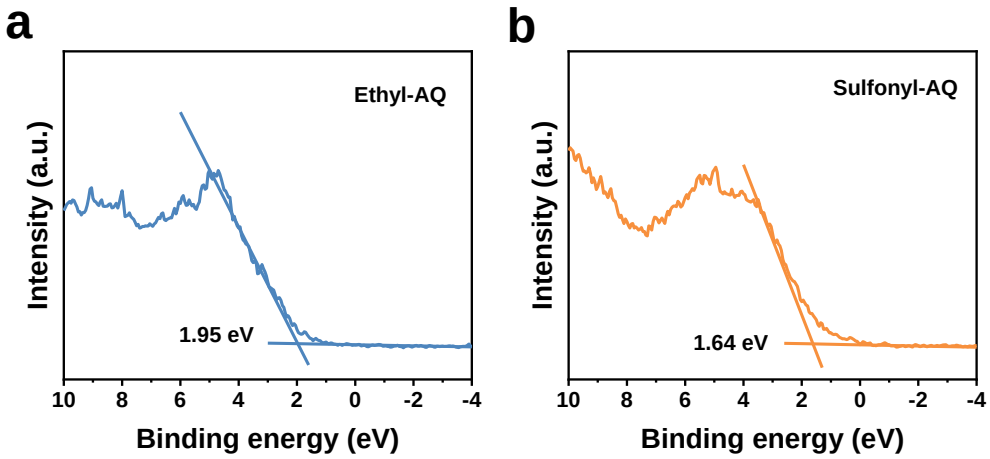

Figure S15. XPS valance band spectra of (a) Ethyl-AQ, (b) Sulfonyl-AQ.

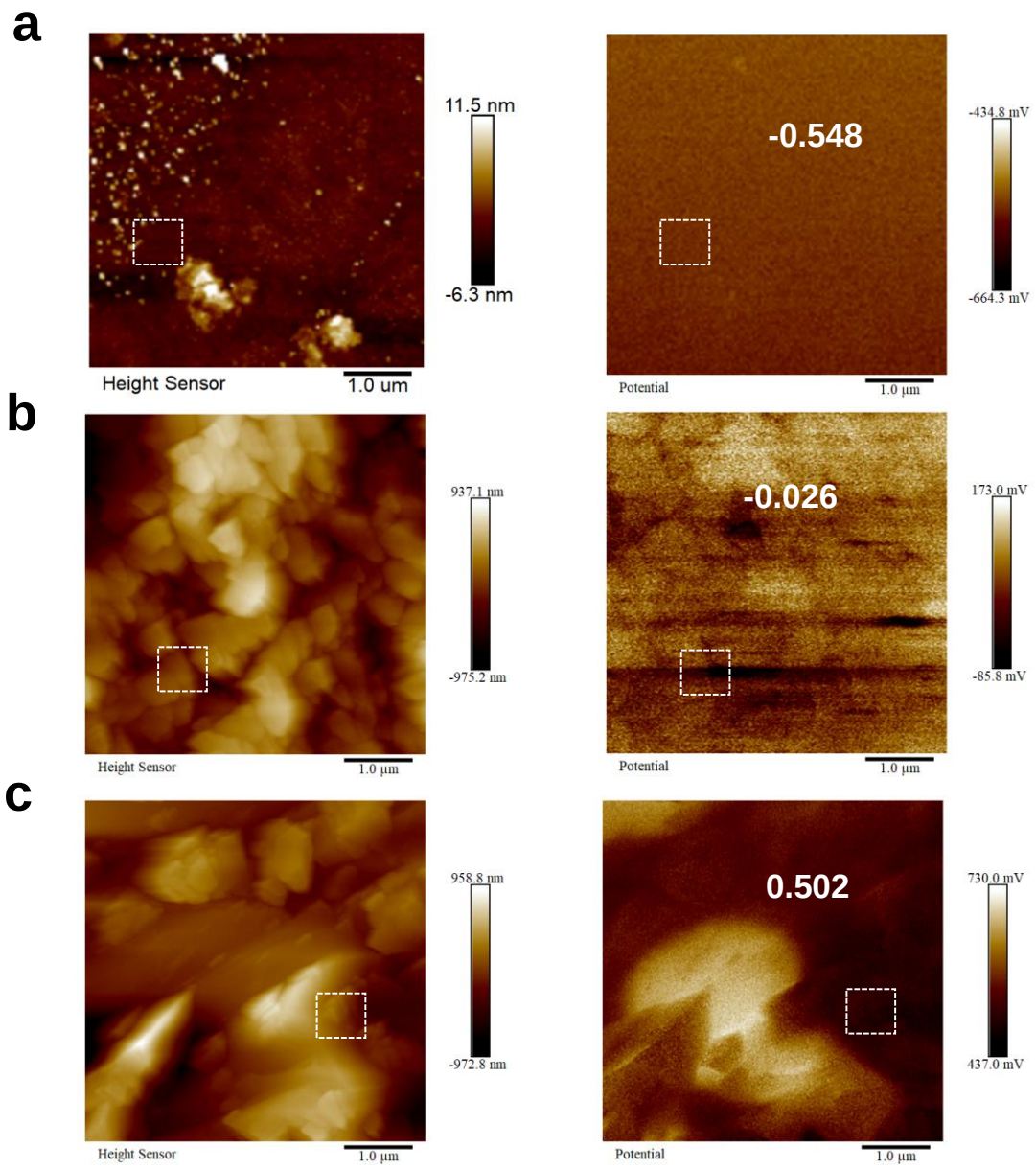

Figure S16. The work function testing with KPFM for (a) Au, (b) Sulfonyl-AQ and (c) Ethyl-AQ. The determination of the work function (φ) involves calibration with a gold standard sample. The work function (φ) is computed using the formula: $\varphi = 5.2 - (V_R - V_{Au})$, where V_R represents the measured potential of the material, and V_{Au} is the potential of the gold standard sample.

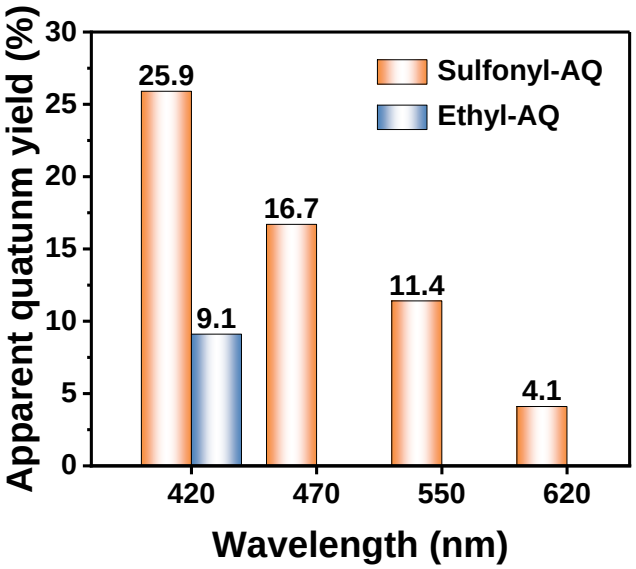

Figure S17. The apparent quantum yields for H_2O_2 generation of Ethyl-AQ and Sulfonyl-AQ at the specified wavelength.

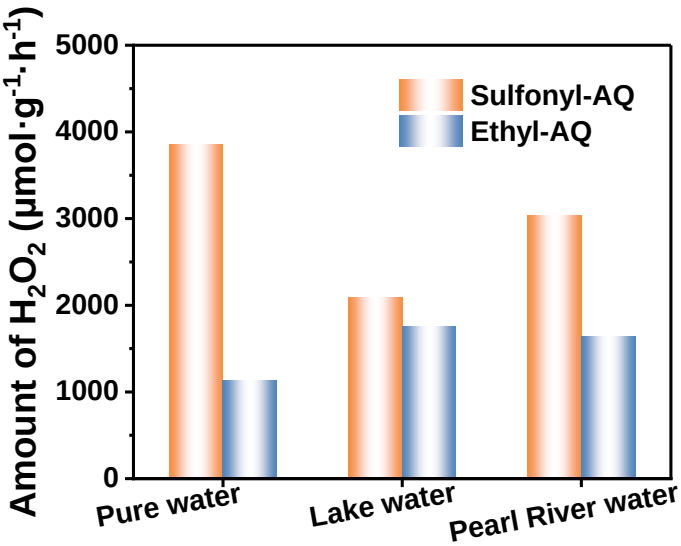

Figure S18. Photosynthetic H_2O_2 production by CPs in pure water, lake water, and the Pearl River over one hour.

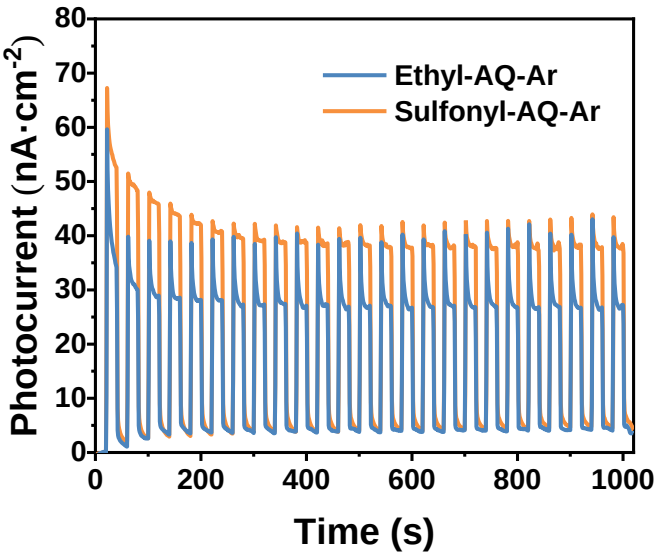

Figure S19. Comparison of transient photocurrent responses for Ethyl-AQ and Sulfonyl-AQ in Ar atmosphere.

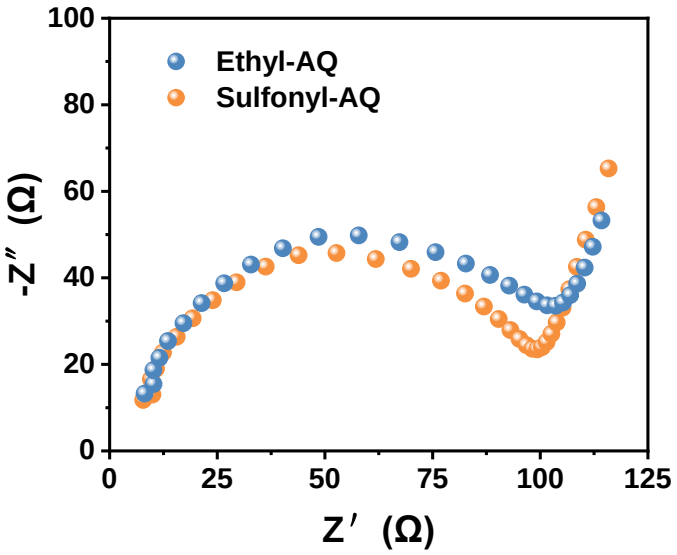

Figure S20. Electrochemical impedance spectra of Ethyl-AQ and Sulfonyl-AQ.

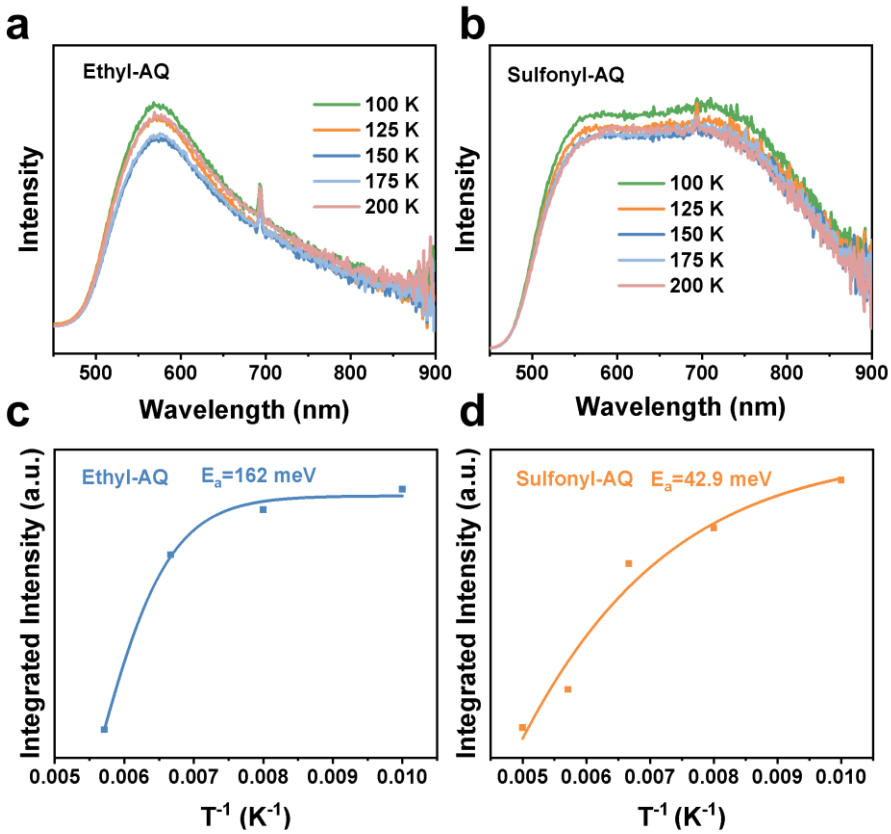

Figure S21. Temperature-dependent PL spectra for (a) Ethyl-AQ and (b) Sulfonyl-AQ. Evolution of PL intensity as a function of temperature from 100 to 200 K for (c) Ethyl-AQ and (d) Sulfonyl-AQ.

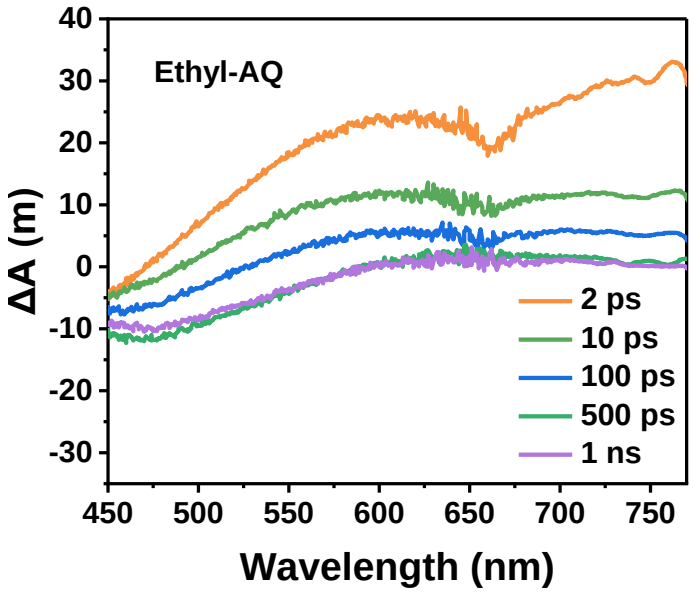

Figure S22. Time slices of the TA spectra for Ethyl-AQ in water.

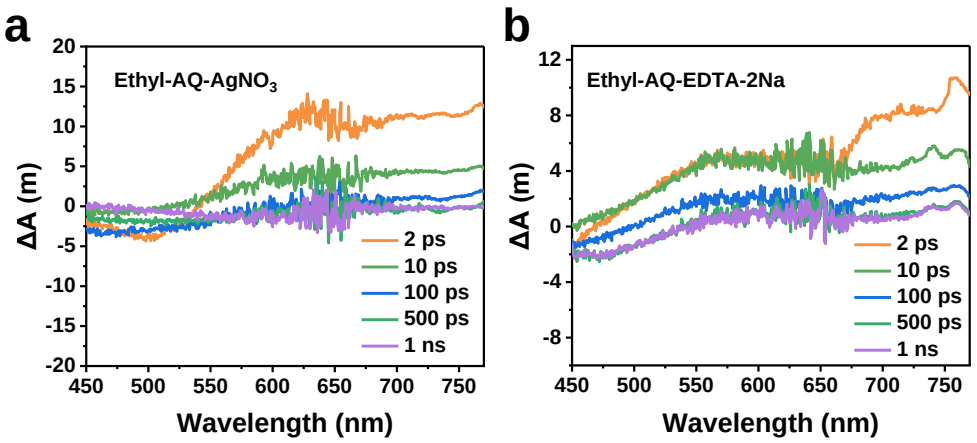

Figure S23. Time slices of the TA spectra for Ethyl-AQ in EDTA-2Na (a) and $AgNO_3$ (b). The concentrations of EDTA-2Na and $AgNO_3$ utilized were both 10 mM.

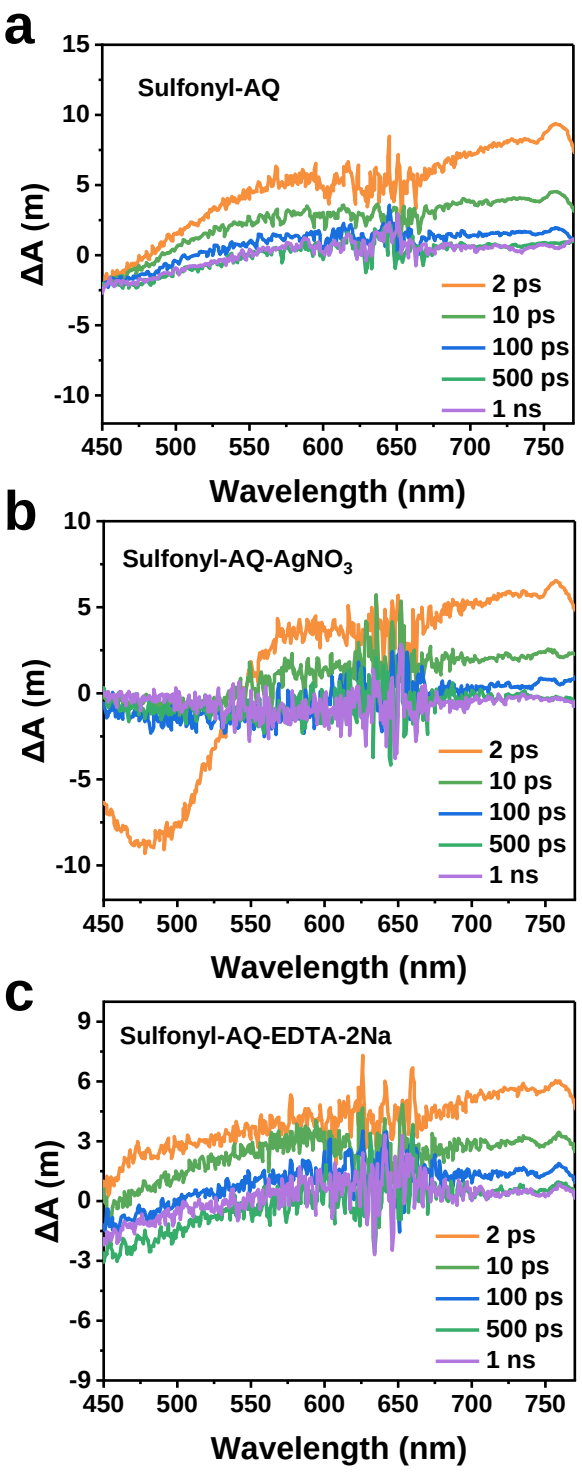

Figure S24. Time slices of the TA spectra for Sulfonyl-AQ in water (a), EDTA-2Na (b) and $AgNO_3$ (c). The concentrations of EDTA-2Na and $AgNO_3$ utilized were both 10 mM.

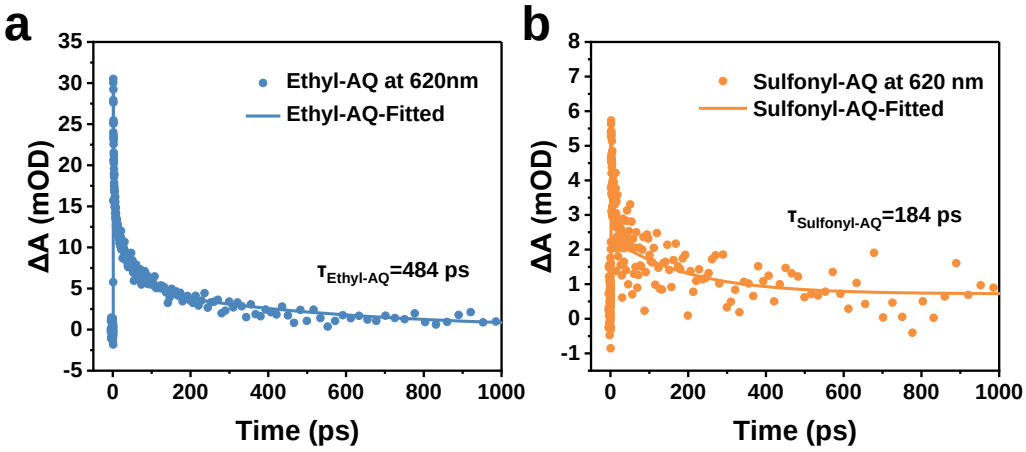

Figure S25. Comparison of the TA kinetics for CPs probed at 620 nm.

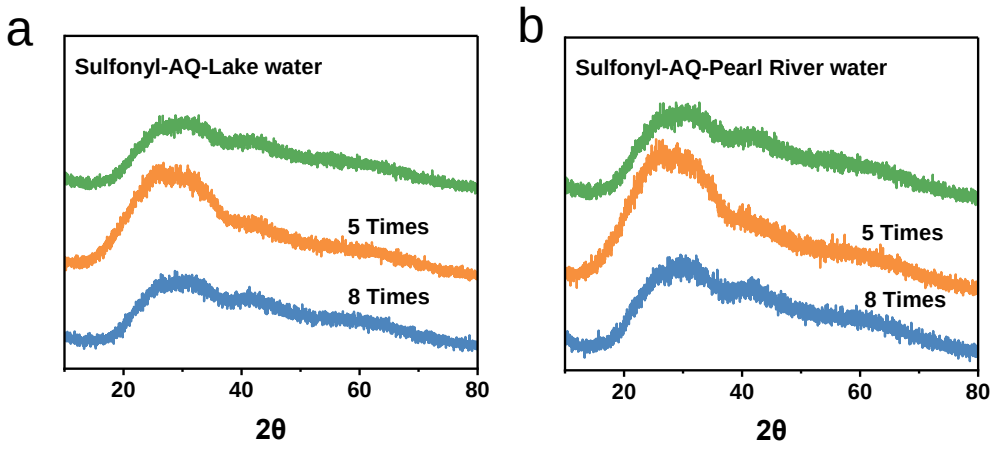

Figure S26. The PXRD patterns of Sulfonyl-AQ in (a) Lake water and (b) Pearl River water before and after 8 times of repeated photocatalytic tests.

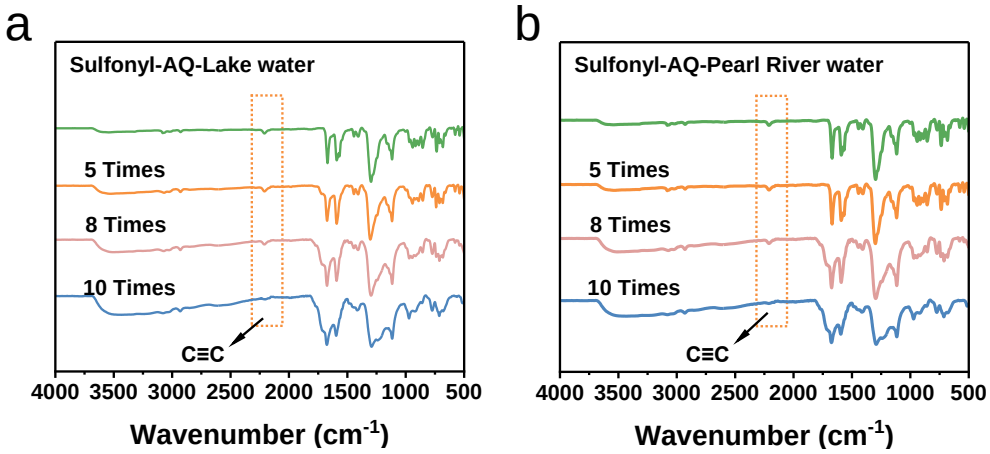

Figure S27. The FT-IR spectra of Sulfonyl-AQ in (a) Lake water and (b) Pearl River water before and after 10 times of repeated photocatalytic tests.

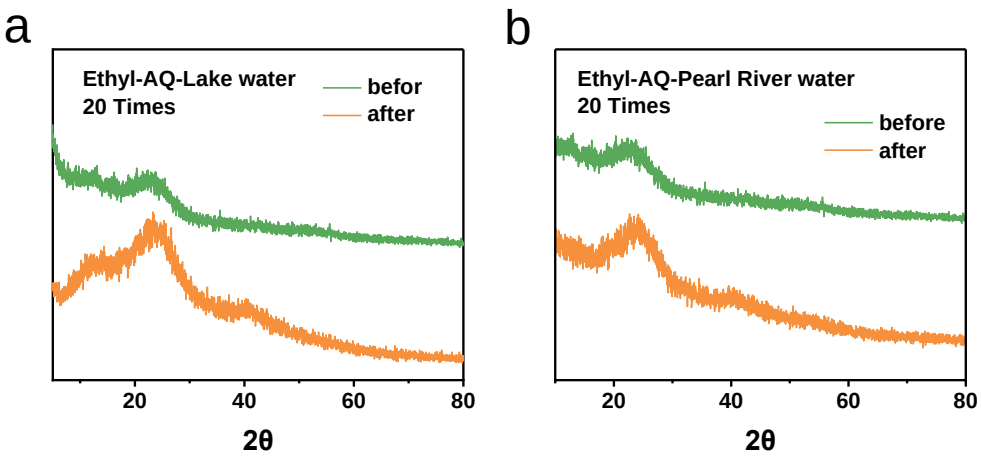

Figure S28. The PXRD patterns of Ethyl-AQ in (a) Lake water and (b) Pearl River water before and after 20 times of repeated photocatalytic tests.

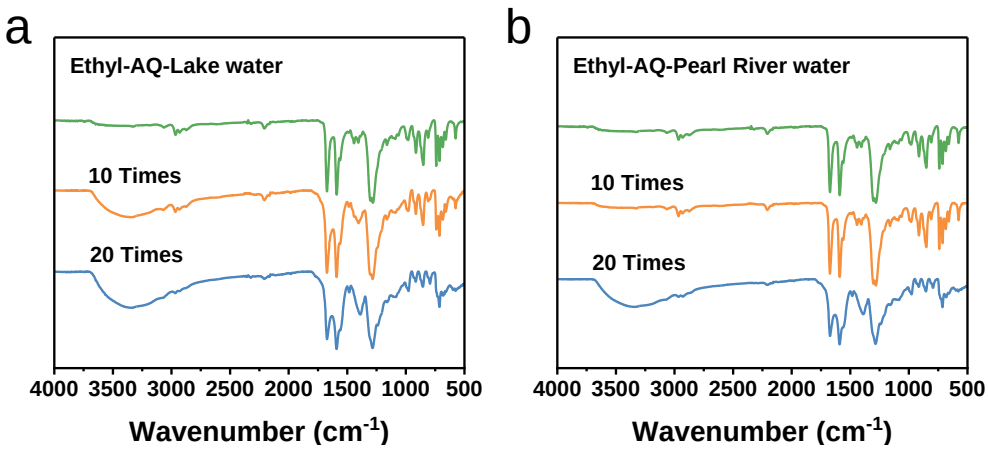

Figure S29. The FT-IR spectra of Ethyl-AQ in (a) Lake water and (b) Pearl River water before and after 10 and 20 times of repeated photocatalytic tests.

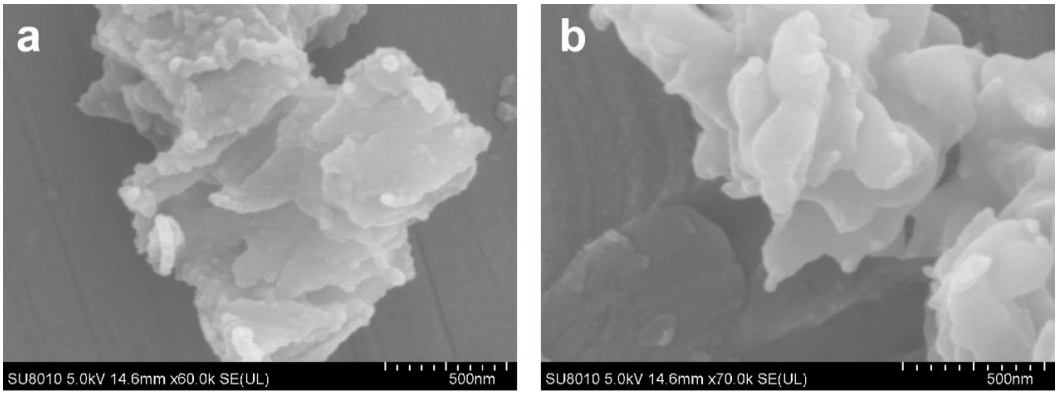

Figure S30. The SEM images of Ethyl-AQ in (a) Lake water and (b) Pearl River water after 20 repeated photocatalytic tests.

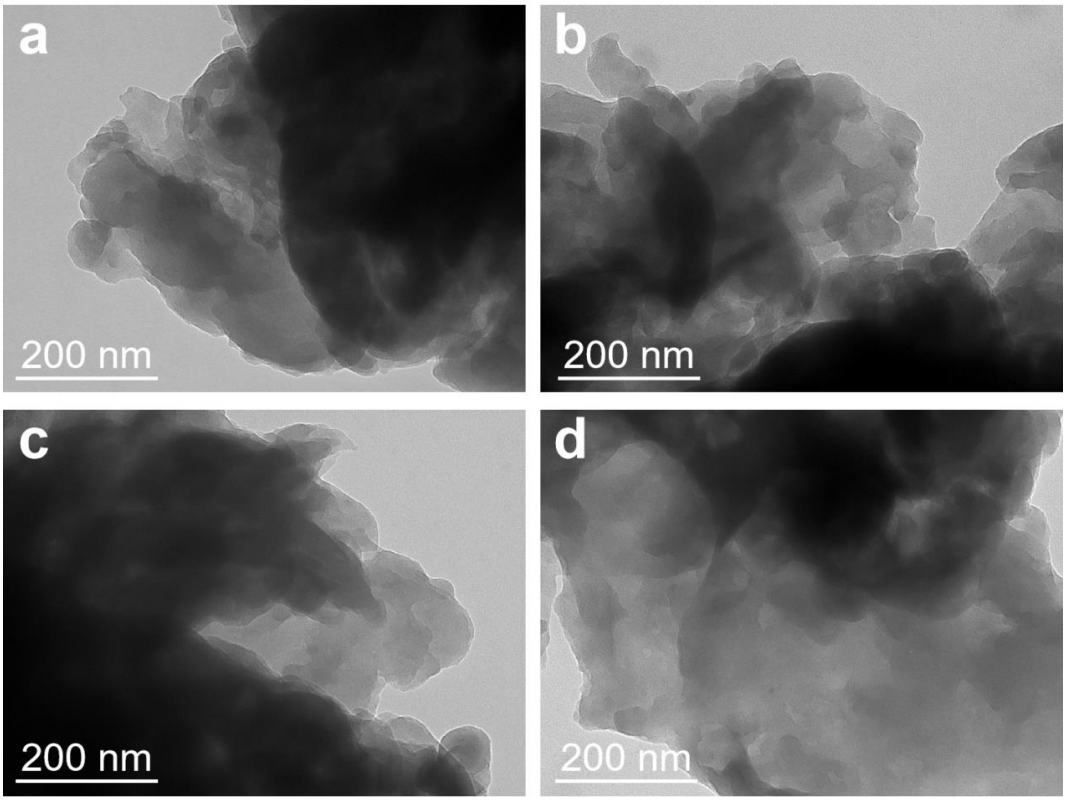

Figure S31. TEM images of Ethyl-AQ before and after 20 cycles: (a) Pre-cycle in lake water; (b) Post-cycle in lake water; (c) Pre-cycle in Pearl River water; (d) Post-cycle in Pearl River water.

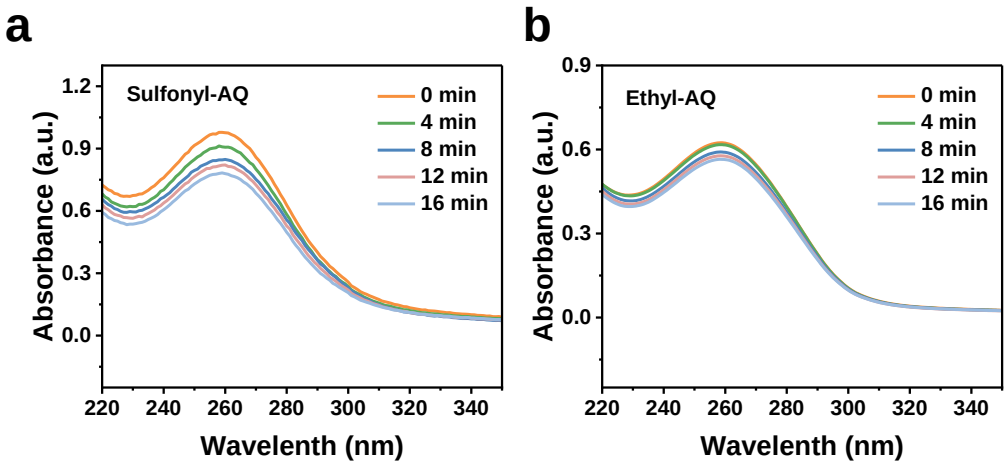

Figure S32. The absorption changes of NBT with (a) Sulfonyl-AQ and (b) Ethyl-AQ. The UV spectra tested after 1 mg of Sulfonyl-AQ and Ethyl-AQ were dispersed in 50 mL of pure water and irradiated with visible light (100 mW·cm^{-2}) for 16 minutes.

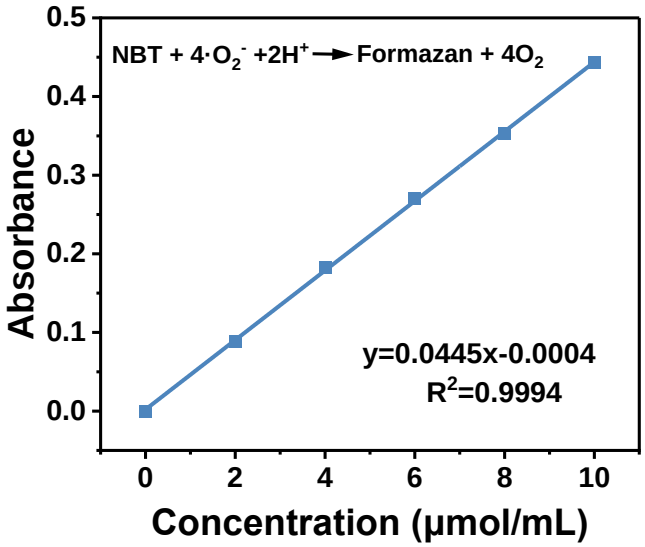

Figure S33. Standard curve of •O_2^-

The concentration of •O_2^- can be quantitatively determined by NBT method.

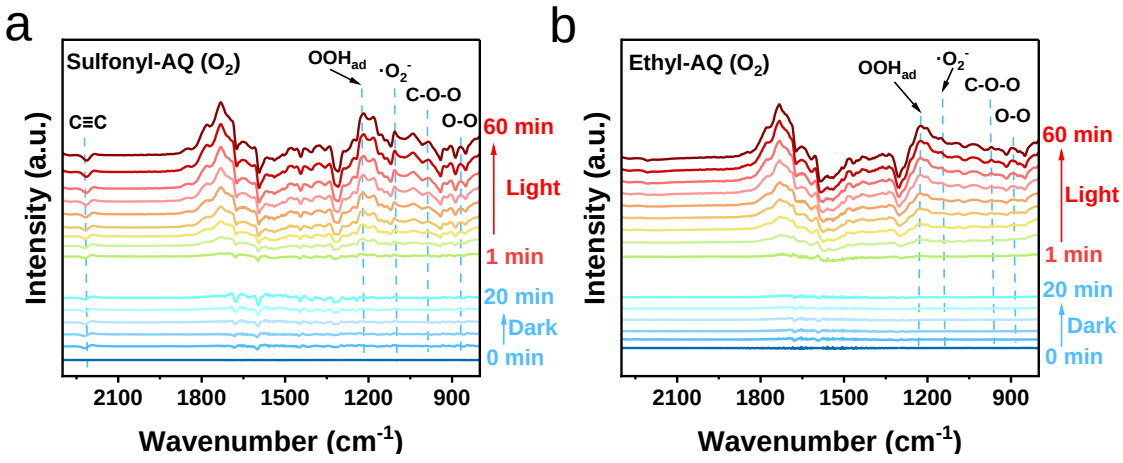

Figure S34. In-situ DRIFTS of Sulfonyl-AQ and Ethyl-AQ under O_2.

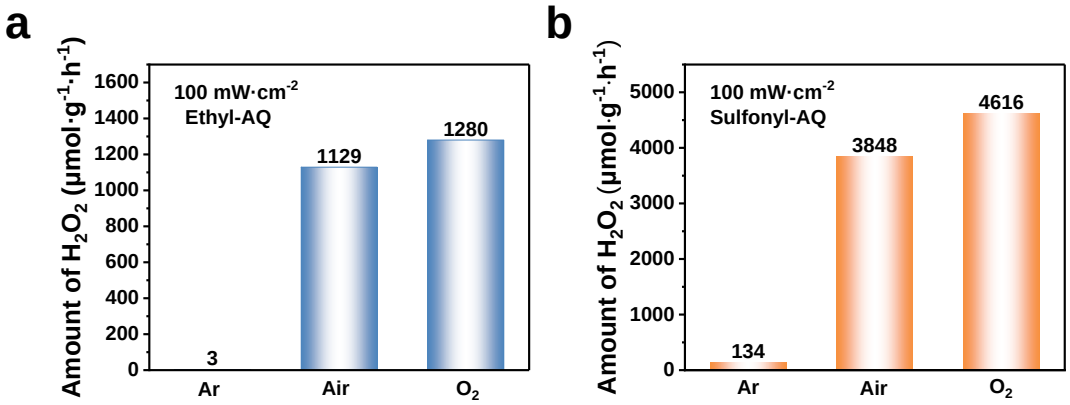

Figure S35. Photocatalytic H_2O_2 production of Ethyl-AQ and Sulfonyl-AQ in Ar, Air and O_2.

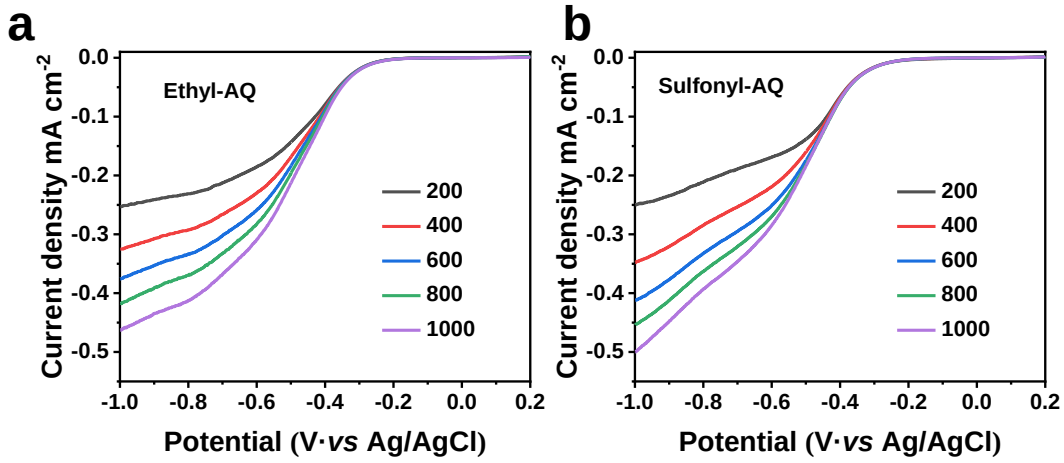

Figure S36. The LSV curves were measured on RDE at different rotating of (a) Ethyl-AQ and (b) Sulfonyl-AQ.

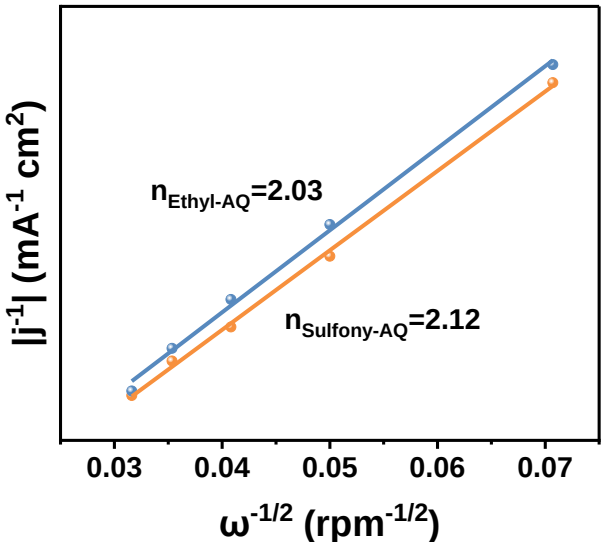

Figure S37. Koutecky–Levich plots obtained by RDE measurements.

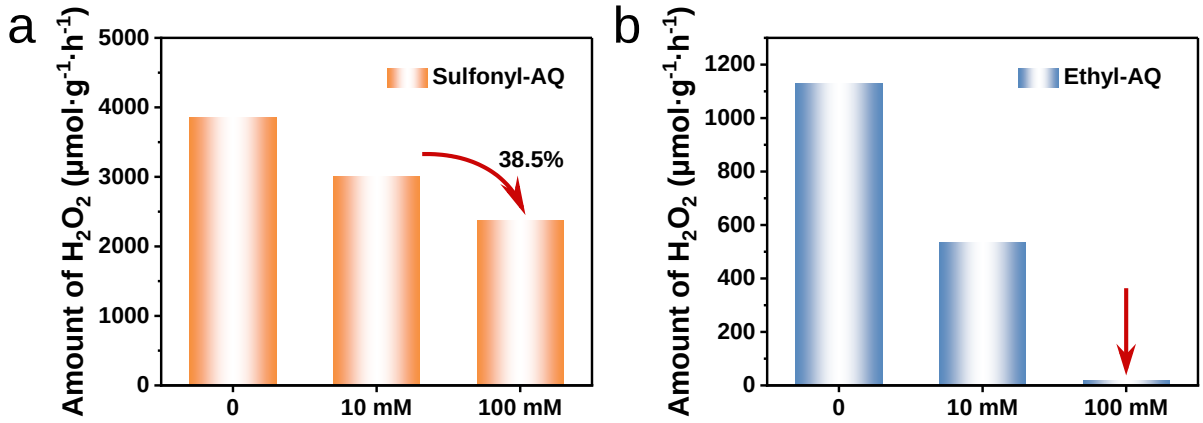

Figure S38. Performance Diagrams of H_2O_2 Production via Photocatalysis with DFO of CPs Quantitatively Varied.

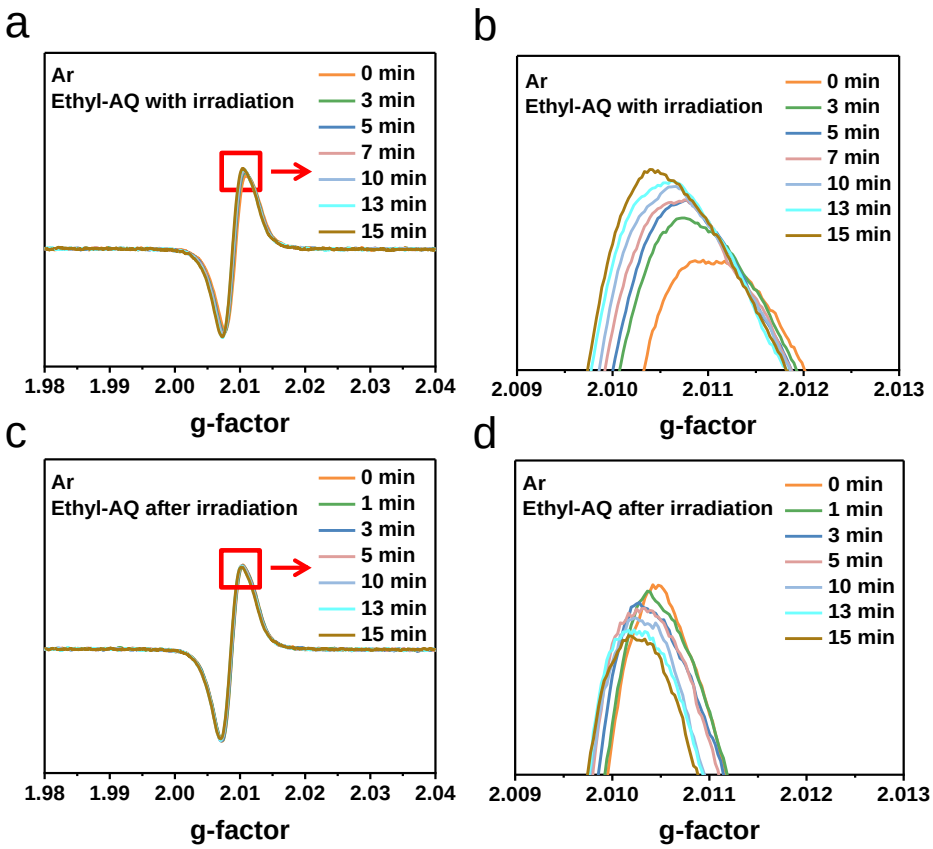

Figure S39. In situ solid-state Electron Paramagnetic Resonance (EPR) spectra of Ethyl-AQ under irradiation conditions. (a) EPR spectra of Ethyl-AQ under irradiation in an argon atmosphere. (b) Magnified view of the EPR peak under irradiation in argon. (c) EPR spectra of Ethyl-AQ after irradiation in argon. (d) Magnified view of the EPR peak after irradiation in argon.

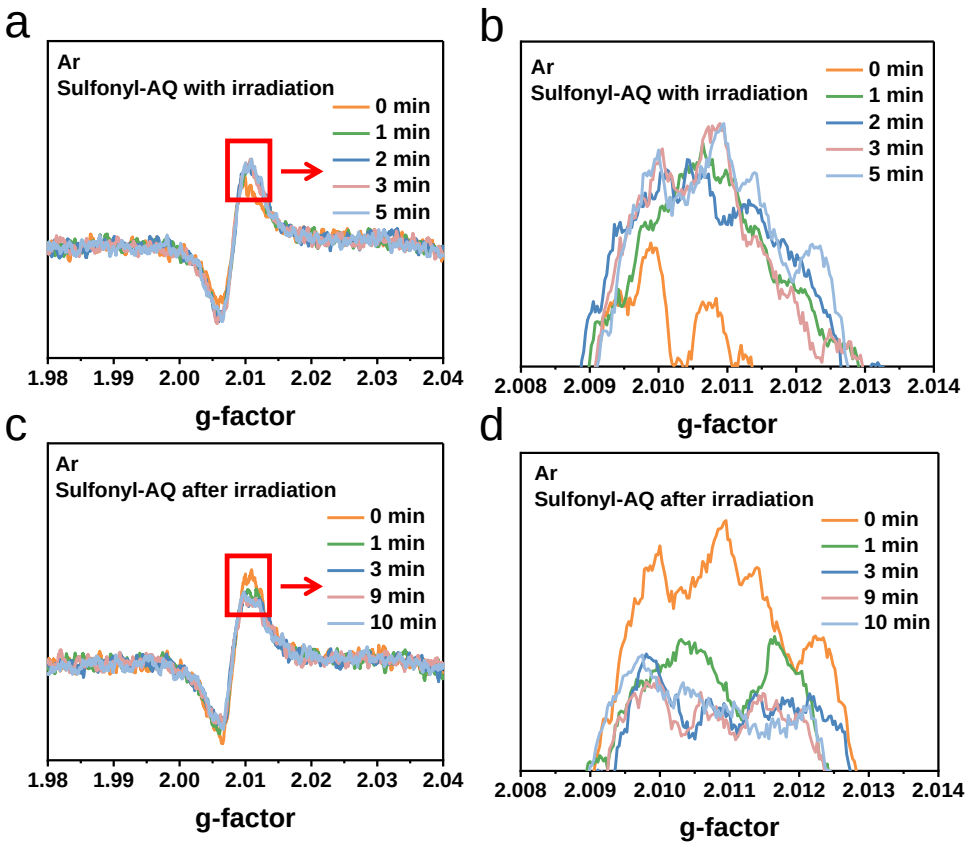

Figure S40. In situ solid-state Electron Paramagnetic Resonance (EPR) spectra of Sulfonyl-AQ under irradiation conditions. (a) EPR spectra of Sulfonyl-AQ under irradiation in an argon atmosphere. (b) Magnified view of the EPR peak under irradiation in argon. (c) EPR spectra of Sulfonyl-AQ after irradiation in argon. (d) Magnified view of the EPR peak after irradiation in argon.

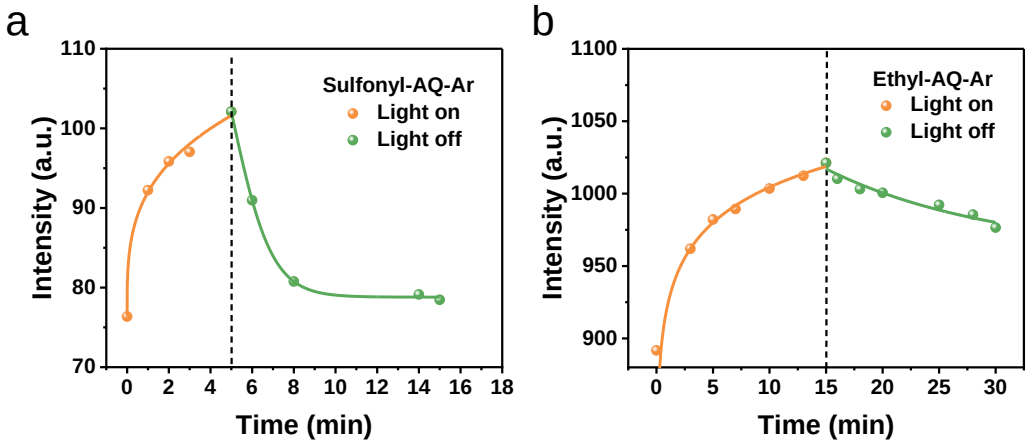

Figure S41. Changes in the highest EPR peak intensity over time in argon after light irradiation and subsequent removal of light exposure: (a) Sulfonyl-AQ, (b) Ethyl-AQ.

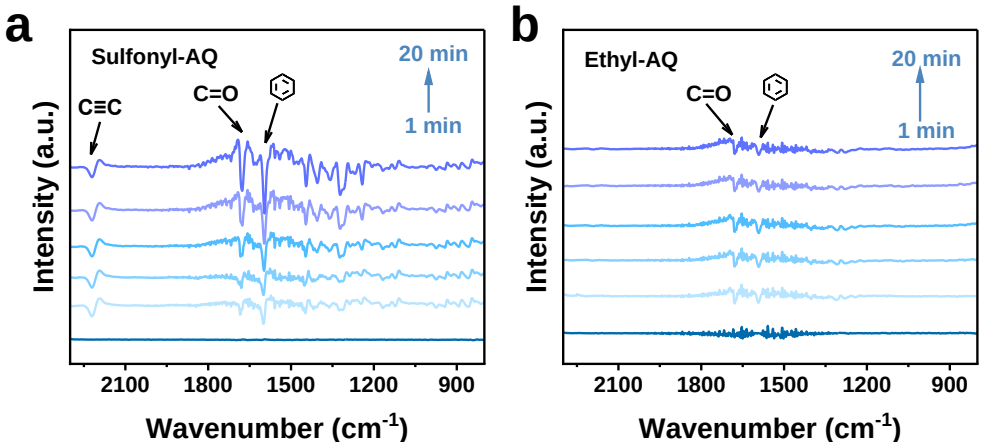

Figure S42. In situ DRIFTS of oxygen adsorption in dark for CPs.

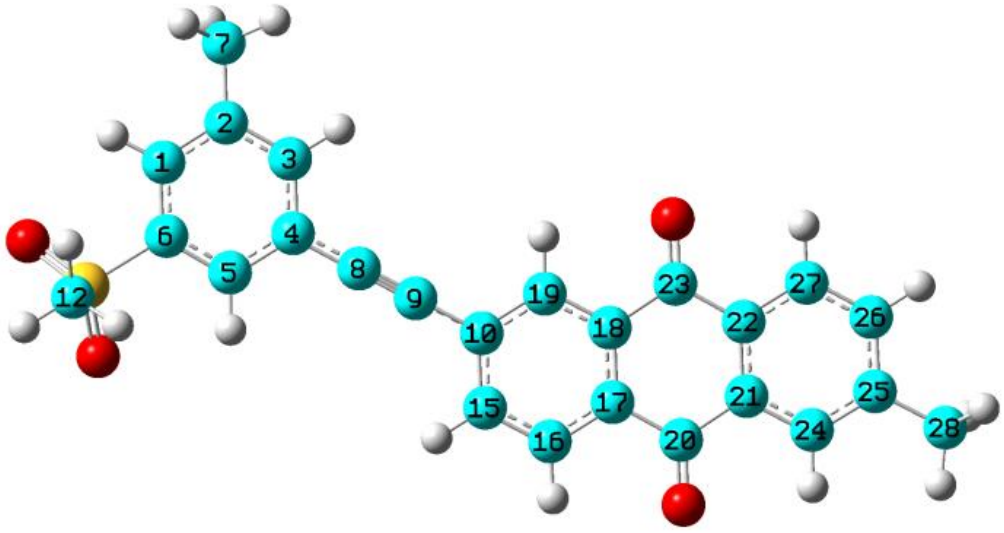

Figure S43. The atom list of Sulfonyl-AQ.

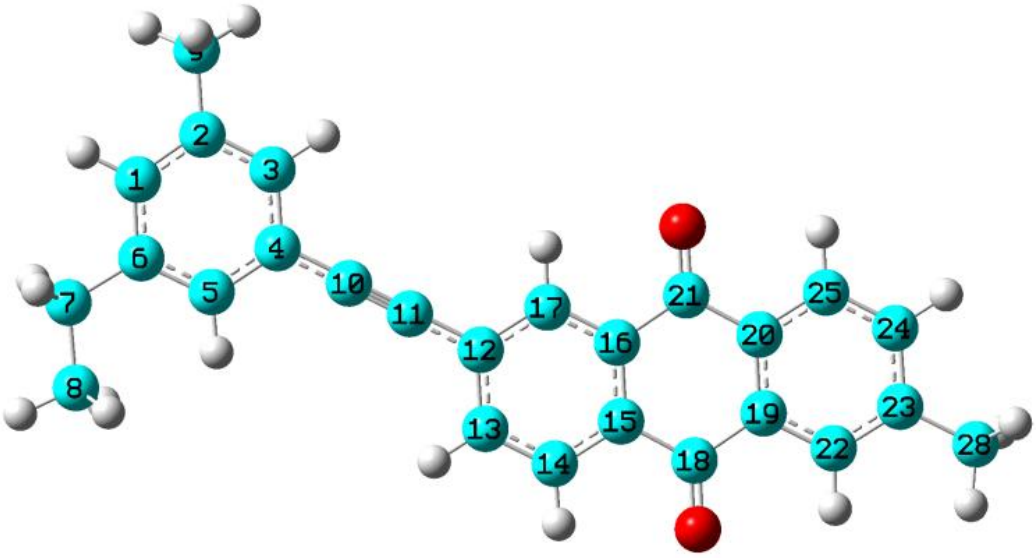

Figure S44. The atom list of Ethyl-AQ.

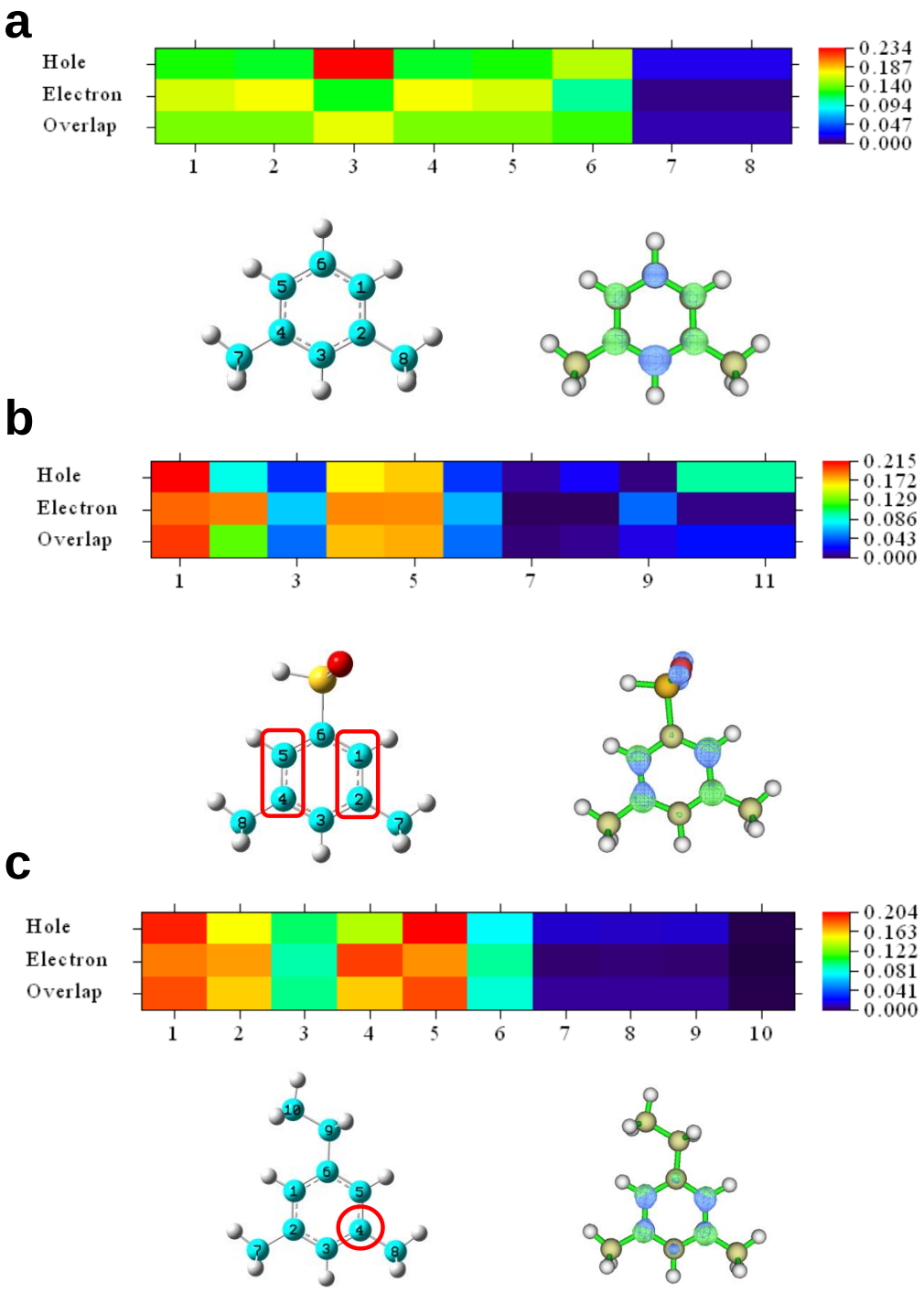

Figure S45. The distribution of electrons (in green) and holes (in blue) is presented. The contribution of non-hydrogen atoms to holes and electrons in excited benzene (a), sulfonyl group (b), and ethyl group (c), along with the corresponding distribution of atomic serial numbers, is shown. The colors represent: C (blue), H (gray), O (red), and S (yellow).

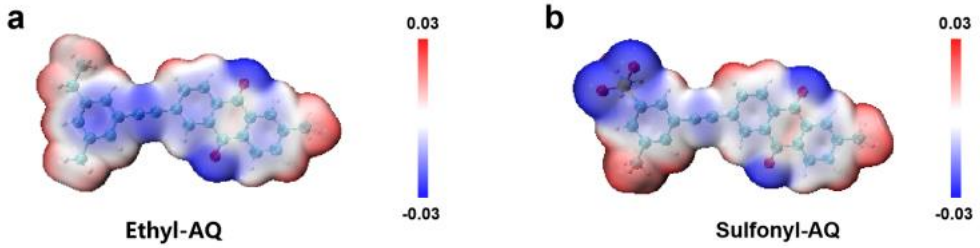

Figure S46. Electrostatic potential (ESP) of Ethyl-AQ (a) and Sulfonyl-AQ (b).

3. Supplementary Tables

Table S1. Brunauer-Emmett-Teller (BET) surface areas of the CPs

	Sulfonyl-AQ	**Ethyl-AQ**
BET Surface ($m^2 \cdot g^{-1}$)	165.09	98.14

Table S2. Solar-to-chemical conversion (SCC) efficiencies for various photocatalytic reactions in recent literature.

Photocatalysts	Conditions		SCC efficiency	Ref.
	Atmosphere	Water body		
TapbBtt	O_2	Pure water	0.297%	[9]
PyIm-COF	O_2	Pure water	0.28%	[10]
BTDB-$CN_{0.2}$	Air	Pure water	0.019 %	[11]
RF/P3HT-1.0	O_2	Pure water	1.0%	[12]
CTF-DPDA	O_2	Pure water	0.78%	[13]
HEP-TAPT-COF	O_2	Pure water	0.65%	[14]

RF-DHAQ-2	O_2	Pure water	1.2%	[15]
SA-TCPP	O_2	Pure water	1.2%	[16]
TTF-BT-COF	O_2	Pure water	0.49%	[17]
CTF-DA-Film-3	O_2	Pure water	0.123%	[18]
PIC-BPY	Air	Pure water	0.22%	[19]
Sulfonyl-AQ	Air	Pure water	1.29%	This work

Table S3. Oscillator strengths of excited states of monomers from Sulfonyl-AQ and Ethyl-AQ.

Excited states	Oscillator strengths	
	Sulfonyl-AQ	Ethyl-AQ
$S_0 \rightarrow S_1$	0.3394	0.3353
$S_0 \rightarrow S_2$	0.0012	0.0000
$S_0 \rightarrow S_3$	0.0000	0.0000
$S_0 \rightarrow S_4$	0.2198	0.0038
$S_0 \rightarrow S_5$	0.0495	0.1259
$S_0 \rightarrow S_6$	0.7344	0.4501
$S_0 \rightarrow S_7$	0.4367	0.3474
$S_0 \rightarrow S_8$	0.0741	0.4008

$S_0 \rightarrow S_9$	0.0111	0.0004
$S_0 \rightarrow S_{10}$	0.0000	0.0862
$S_0 \rightarrow S_{11}$	0.0895	0.0164
$S_0 \rightarrow S_{12}$	0.0040	0.1665
$S_0 \rightarrow S_{13}$	0.0482	0.0000
$S_0 \rightarrow S_{14}$	0.1633	0.3036
$S_0 \rightarrow S_{15}$	0.0000	0.0001
$S_0 \rightarrow S_{16}$	0.0602	0.0000
$S_0 \rightarrow S_{17}$	0.0031	0.0401
$S_0 \rightarrow S_{18}$	0.0022	0.0000
$S_0 \rightarrow S_{19}$	0.0187	0.0030
$S_0 \rightarrow S_{20}$	0.0687	0.0145

[1] S. Grimme, J. Antony, S. Ehrlich,H. Krieg，*J.Chem.Phys.* **2010,** *132,* 154104.

[2] R. Krishnan, J.S. Binkley, R. Seeger,J.A. Pople，*J.Chem.Phys.* **1980,** *72,* 650-654.

[3] F.J.D. P. J. Stephens，*Physical Chemistry* **1994,** *98,* 11623–11627.

[4] B. Machura, I. Gryca, J.G. Małecki, F. Alonso,Y. Moglie，*Dalton Trans.* **2014,** *43,* 2596-2610.

[5] Z. Liu, T. Lu,Q. Chen，*Carb.* **2020,** *165,* 461-467.

[6] T. Lu,F. Chen，*J.Comput.Chem.* **2011,** *33,* 580-592.

[7] L. Zhang, Y. Huang, H. Yan, Y. Cheng, Y.X. Ye, F. Zhu,G. Ouyang，*Adv. Mater.* **2024,** *36,* 2401162.
[8] W. Zheng, T. Yang, L. Qu, X. Liang, C. Liu, C. Qian, T. Zhu, Z. Zhou, C. Liu, S. Liu, Z. Chi, J. Xu,Y. Zhang，*Chem. Eng. J.* **2022,** *436,* 135060.
[9] X.W. Chencheng Qin, Lin Tang, Xiaohong Chen, MiaoLi, Yi Mou,BoSu,SiboWang, Chengyang Feng, Jiawei Liu, Xingzhong Yuan , Yanli Zhao, Hou Wang，*Nat. Commun.* **2023,** *14,* 5238.
[10] W. Wu, Z. Li, S. Liu, D. Zhang, B. Cai, Y. Liang, M. Wu, Y. Liao,X. Zhao，*Angew. Chem. Int. Ed.* **2024,** *63,* e202404563.
[11] J. Cheng, W. Wang, J. Zhang, S. Wan, B. Cheng, J. Yu,S. Cao，*Angew. Chem. Int. Ed.* **2024,** *63,* e202406310.
[12] Y. Shiraishi, M. Matsumoto, S. Ichikawa, S. Tanaka,T. Hirai，*J. Am. Chem. Soc.* **2021,** *143,* 12590-12599.
[13] H. Cheng, H. Lv, J. Cheng, L. Wang, X. Wu,H. Xu，*Adv. Mater.* **2021,** *34,* 2107480.
[14] D. Chen, W. Chen, Y. Wu, L. Wang, X. Wu, H. Xu,L. Chen，*Angew. Chem. Int. Ed.* **2023,** *62,* e202217479.
[15] C. Zhao, X. Wang, Y. Yin, W. Tian, G. Zeng, H. Li, S. Ye, L. Wu,J. Liu，*Angew. Chem. Int. Ed.* **2023,** *62,* e202218318.
[16] Y. Zhang, C. Pan, G. Bian, J. Xu, Y. Dong, Y. Zhang, Y. Lou, W. Liu,Y. Zhu，*Nat. Energy* **2023,** *8,* 361-371.
[17] J.N. Chang, Q. Li, J.W. Shi, M. Zhang, L. Zhang, S. Li, Y. Chen, S.L. Li,Y.Q. Lan，*Angew. Chem. Int. Ed.* **2023,** *62,* e202218868.
[18] Y. Guo, X. Yang, R. Sun, X. Hu, C. Shu, X. Yang, H. Gao, X. Wang,B. Tan，*Sm.* **2024,** *20,* 2403743.
[19] T. Kim, D.-Y. Lee, E. Choi, H.-i. Kim,B.-S. Kim，*Appl. Catal. B: Environ. Energy* **2024,** *357,* 124264.